S1_supplemental material

for

Chemogenetic E-MAP in *Saccharomyces cerevisiae* for identification of membrane transporters operating lipid flip flop

Hector M. Vazquez*, Christine Vionnet*, Carole Roubaty*, Shamroop Mallela*, Roger Schneiter* and Andreas Conzelmann*§

The MSP- and MSP/C-EMAPs showed the well-known characteristics described for other yeast E-MAPs

1) High profile correlations connect functionally related genes.

In 22 amongst the 68 gene pairs with correlation scores >0.5 in the MSP- or MSP/C-E-MAP (listed in S2C Table), both genes of the pair are involved in N-glycosylation. In a further 6 out of 11 gene pairs involving mitochondrial genes in S2C Table both partners are required for mitochondrial respiration and their S scores are all positive. Other examples of correlations >0.5 concern the functionally related pairs *CHS3-CHS7* required for chitin synthesis and *BST1-PER1* involved in GPI anchor remodeling (S2C Table, see below).

2) Hierarchical clustering based on less strong profile correlations also clusters functionally related genes together.

Hierarchical clustering of the 543 genes of the MSP-E-MAP based on the similarity of their correlations (see S3_supplemental material, materials and methods) generated the heat maps of S8 Fig, for which the starting, non-clustered matrices are shown in S4A, S4B Tables, whereas the resulting clustered matrices are shown in S3A and S3B Tables, respectively. The result of hierarchical clustering shown in S8 Fig demonstrates that hierarchical clustering brings together genes working for similar functions even if their profile correlations are lower than 0.4.

Cluster 1 of S8A Fig groups together genes for protein glycosylation and cell wall biosynthesis. Cluster 1 in S8A Fig contains genes involved in N-glycosylation, which interact negatively with each other, causing the green coloring next to the diagonal. Blow up of this cluster (S8C Fig) shows that genes are subdivided in two sub-clusters consisting of a) those that build the dolichol-linked oligosaccharide (*ALG8* to *DIE2*) and b) the subunits of the oligosaccharyltransferase (OST)(*OST3* to *SWP1*) that transfers the oligosaccharide to nascent substrate proteins in the ER as described before [1]. As expected, deletions in the

former sub-cluster are epistatic and result in no or positive genetic interactions between each other, but deletions in the former sub-cluster interact very negatively with deletions of OST subunits of the second sub-cluster. This recapitulates the well-known fact that the defect caused by a crippled OST is enhanced, when it has to transfer a crippled oligosaccharide. Within the OST deletions, some pairs are neutral, but some result in very negative interactions as well. Cluster 1 also contains *GUP1* and *KRE1*, required respectively for GPI protein remodeling and β-glucan biosynthesis, processes which, together with N-glycosylation, collaborate for cell wall integrity (CWI) [2,3]. *GUP1* and *KRE1* however are the only genes of cluster 1 to also have a high number of negative and positive interactions outside of cluster 1 and throughout the heat-map, suggesting that they have a greater impact on cell growth than N-glycosylation. Several of the genes involved in GPI or cell wall glucan biosynthesis of cluster 1 (*GUP1, LAS21, ARV1* and *KRE1*) interact also negatively with *CCH1, CHS3, CHS7, ERG3*, and *OST6* of cluster 4 (see below), which are equally required for CWI (S8A Fig, box 1γ). Thus, genes required for CWI are split up between clusters 1 and 4.

Cluster 5 of S8A Fig contains mitochondrial genes, which frequently interact with genes in other functional categories. The diagonal of S8A Fig also highlights cluster 5, most genes of which are required for mitochondrial respiration. These genes interact positively with each other, as expected, but they also interact with a great number of other genes far from the diagonal, highlighted by boxes 1δ, 5η, and 5θ. Thus, genes of cluster 5 contain frequent interactions with several genes of cluster 1 required for cell wall integrity (CWI) (*BST1, GUP1, KRE1, ARV1, ALG6*)(box 1δ). The positive interactions of box 1δ may suggest that the slow growth phenotype of respiration deficient mutants (*PAM17, MGR2, TIM17*) makes cell wall biosynthesis less important, but this seems to be the case only in certain conditions because other non-respiring mutants of cluster 5 don't show these positive interactions, and since *GPI2* and *GPI13*, two other genes affecting cell wall biosynthesis, interact negatively with cluster 5 genes. Intriguingly, most genes in the mitochondrial cluster 5 show strong negative interactions with the hyper-interactor *SUR1* (=*CSG1*), required for mannosyl-phosphorylinositolceramide biosynthesis and with *AUS1*, a lipid flippase at the plasma membrane, although none of these interactions is reported in BIOGRID (S9 Fig).

3) Hierarchical clustering often brings together functionally related genes, which amongst themselves show no major genetic interactions but only correlations.

Such is the case for clusters 2 – 4 and 6, which appear as blue regions along the diagonal in S8B Fig, but are not very colorful in S8A Fig and S8C Fig. They get clustered together because of the similarity of their genetic interactions with other genes, reflected by strong blue color far from the diagonal.

Cluster 2 contains the *DFG16*/*RIM9* pH sensor complex, whereby deletion of either one destroys the sensing function. This results in the expected picture of high correlation and also a positive genetic interaction of *dfg16*Δ and *rim9*Δ mutations (enlarged in S8C Fig).

Cluster 3 contains many transporters but also genes with other functions and interacts quite negatively with the mitochondrial respiration genes of cluster 5 (S8A Fig, box 5η, S9 Fig).

Cluster 6 of S8B Fig seems to be functionally heterogeneous, but appears as the epicenter of a larger cluster grouping genes, positively correlated not only amongst themselves but also with groups far from the diagonal (S8B Fig, boxes α, 2ζ, 5θ). Only boxes β and 5θ, i.e. the *ELO2/CCC2/FTR1* microcluster and the mitochondrial respiration genes of cluster 5 interact genetically with the cluster 6 genes (S8A Fig). Also visible in S8B Fig, pairs combining genes from cluster 6 with genes from clusters 3 or 4 show negative correlations (grey zones).

4) Interactions amongst different functional classes.

Instead of letting the hierarchical clustering bring together functionally related genes, we inverted the process by first grouping our 543 E-MAP genes into 11 classes according to the biological process annotations as described in S1 Table and reflected in the color codes of S8C Fig and then interrogating the data for the frequency of interactions and correlations within classes and between different classes. S10A Fig shows a high tendency for negative interactions and positive correlations within the group of genes acting in protein maturation/targeting (purple). To a lesser degree this also is true for genes involved in biosynthesis of the cell wall (red). Protein maturation and cell wall biosynthesis genes also strongly interact with each other in that there are frequent negative interactions combined with positive correlations between genes of these two classes S10A Fig. Within the class of mitochondrial genes (cyan) there is a tendency to have positive genetic interactions and positive correlations reflected in S8A Fig by cluster 5. Corresponding boxes in S8 Fig mirror all these elevated interaction and correlation frequencies.

5) Statistical analysis of E-MAPs.

Not having performed E-MAPs before, we have undertaken some statistical analysis of our E-MAPs, which were certainly done but not necessarily reported for previous E-MAPs. One approach was to compare the 543 genes of the E-MAP set with each other rather than compare pairs of genes to each other. As can be seen from S11A and S11D Fig, in the MSP-E-MAP, genes generated an average of 1.6 positive and 1.1 negative significant interactions and of 1.85 positive and 1.1 negative significant correlations. Yet, some genes were found to be involved in significant interactions much more frequently than others, with 5 of the 8 top runners being involved in lipid biosynthesis (*GUP1, SAC1, ELO3, SUR1 (=CSG1), ERG3*), confirming findings of previous high throughput reports [1,4-6] (S11A Fig, S5 Table). These genes are visible on S8A Fig as colored lines, especially if their interactions are not distributed randomly but segregate into regions where positive, others where negative interactions predominate, as is the case for *GUP1*/*KRE1*. Amazingly, *ILM1,* one of the most interactive genes (S11A Fig), has not been functionally characterized. The *ELO3/SAC1* microcluster is not part of cluster 1 but forms multiple positive and negative interactions with *ALG* genes of cluster 1 as can be seen in the enlarged regions of S8C Fig (and throughout the heat map), pointing not yet understood functional interactions between lipid biosynthesis and N-glycosylation. Similarly, the microcluster of *ELO2/CCC2/FTR1* with the later two transporting copper and iron, respectively, is negatively interacting with a total of 19 genes ($P<0.005$), 15 of which are clustered in boxes 2ε and β. The existence of such "hyper-interactors" is also visible when one considers the sum of the significant S scores rather than the number of significant interactions each gene deletion is generating (S11B Fig). Moreover, there is a positive correlation between the number of interactions and the number of correlations each gene generates (S11F Fig), the strongest correlation being the one between the number of negative interactions and the number of positive correlations (S11C Fig). In spite of these tendencies there were 38 genes making no genetic interactions of which 25 still made correlations, and there also were 125 genes not making any correlations but only interactions (S11E Fig).

References for S1_supplemental materials

1. Schuldiner M, Collins SR, Thompson NJ, Denic V, Bhamidipati A, Punna T, et al. Exploration of the Function and Organization of the Yeast Early Secretory Pathway through an Epistatic Miniarray Profile. Cell. 2005;123: 507–519. doi:10.1016/j.cell.2005.08.031

2. Bosson R, Jaquenoud M, Conzelmann A. GUP1 of Saccharomyces cerevisiae encodes an O-acyltransferase involved in remodeling of the GPI anchor. Mol

Biol Cell. 2006;17: 2636–2645. doi:10.1091/mbc.E06-02-0104

3. Boone C, Sommer SS, Hensel A, Bussey H. Yeast KRE genes provide evidence for a pathway of cell wall beta-glucan assembly. J Cell Biol. 1990;110: 1833–1843.

4. Jonikas MC, Collins SR, Denic V, Oh E, Quan EM, Schmid V, et al. Comprehensive characterization of genes required for protein folding in the endoplasmic reticulum. Science. 2009;323: 1693–1697. doi:10.1126/science.1167983

5. Costanzo M, Baryshnikova A, Bellay J, Kim Y, Spear ED, Sevier CS, et al. The genetic landscape of a cell. Science. American Association for the Advancement of Science; 2010;327: 425–431. doi:10.1126/science.1180823

6. Hoppins S, Collins SR, Cassidy-Stone A, Hummel E, Devay RM, Lackner LL, et al. A mitochondrial-focused genetic interaction map reveals a scaffold-like complex required for inner membrane organization in mitochondria. The Journal of Cell Biology. 2011;195: 323–340. doi:10.1083/jcb.201107053

S2_supplemental material

for

Chemogenetic E-MAP in *Saccharomyces cerevisiae* for identification of membrane transporters operating lipid flip flop

Hector M. Vazquez*, Christine Vionnet*, Carole Roubaty*, Shamroop Mallela*, Roger Schneiter* and Andreas Conzelmann*§

Mis en forme : Interligne : 1.5 ligne

Difference between E-MAPs generated in presence and absence of Cerulenin

As shown in S12A Fig, the majority of genetic interactions were quite similar whether or not Cerulenin was present during the last selection, and the correlation between S scores in MSP- and MSP/C-E-MAP was even higher than between replicates 1 and 2 (Fig 1F, 1G). Yet, as seen in S12A Fig, a minority of interactions became less sick (red dots), or sicker on Cerulenin (green dots). Similarly, when comparing the performance of individual genes in the E-MAP without and with Cerulenin, the numbers of significant positive and negative interactions and of positive correlations were positively correlated and in particular the number of negative interactions was highly correlated (R = 0.9) ~~(S13 Fig) ?A 'not shown' possible?~~. Strong interactions were very reproducible in MSP- and MSP/C-E-MAPs (Fig 1F, 1G) suggesting that also the changes leading to appearance or disappearance of such strong S scores on Cerulenin were significant. Gene pairs showing such strong changes are listed in S2E Table and are 4 fold enriched in genes required for lipid biosynthesis and >6 fold in genes for GPI/cell wall biosynthesis. *Elo3*Δ, *sac1*Δ, *per1*Δ and *bst1*Δ were present in both, pairs having much lower as well as pairs having much higher S scores on Cerulenin (S2E Table).

~~?A is this still true?~~

S3_Supplementary material

for

Chemogenetic E-MAP in *Saccharomyces cerevisiae* for identification of membrane transporters operating lipid flip flop

Hector M. Vazquez*, Christine Vionnet*, Carole Roubaty*, Shamroop Mallela*, Roger Schneiter* and Andreas Conzelmann*§

Lists of strains, plasmids and primers

Yeast strains

Strain name	Genotype	Source
BY4741	*MAT*a *his3Δ1 leu2Δ0 met15Δ0 ura3Δ0*	Euroscarf
BY4742	*MAT*α *his3Δ1 leu2Δ0 lys2Δ0 ura3Δ0*	Euroscarf
Euroscarf deletion library (Array)	*MAT*a *his3Δ1 leu2Δ0 met15Δ0 ura3Δ0 xxxXΔ::KanMX4*	Euroscarf
DAmP library (Array)	*MAT*a *his3Δ1 leu2Δ0 met15Δ0 ura3Δ0 xxxX-DAmP-KanMX4*	[1]
y8205	*MAT*α *can1Δ::STE2pr-Sp_his5 lyp1Δ::STE3pr-LEU2 his3Δ1 leu2Δ0 ura3Δ0*	C. Boone
ura3::caURA3MX4	*MAT*α *can1Δ::STE2pr-Sp_his5 lyp1Δ::STE3pr-LEU2 his3Δ1 leu2Δ0 ura3::caURA3MX4*	[2]
MSP-E-MAP queries	*MAT*α *can1Δ::STE2pr-Sp_his5 lyp1Δ::STE3pr-LEU2 his3Δ1 leu2Δ0 ura3Δ0 yyyYΔ::caURA3MX4*	This study
MSP-E-MAP double mutants	*MAT*a *can1Δ::STE2pr-Sp_HIS5 lyp1Δ::STE3pr-leu2 his3Δ1 leu2Δ0 ura3Δ0 xxxXΔ::KanMX4* yyyYΔ::caURA3MX4	This study
*flc1*Δ	*MAT*α *can1Δ::STE2pr-Sp_his5 lyp1Δ::STE3pr-LEU2 his3Δ1 leu2Δ0 ura3Δ0 flc1Δ::caURA3MX4*	This study
*flc2*Δ	*MAT*α *can1Δ::STE2pr-Sp_his5 lyp1Δ::STE3pr-LEU2 his3Δ1 leu2Δ0 ura3Δ0 flc2Δ::NatMX4*	This study

*flc3*Δ	*MAT*a *his3Δ1 leu2Δ0 met15Δ0 ura3Δ0 flc3*Δ*::KanMX4*	Euroscarf
*yor365c*Δ	*MAT*a *his3Δ1 leu2Δ0 met15Δ0 ura3Δ0 yor365c*Δ*::HisMX4*	This study
*flc1*Δ *flc2*Δ	*MAT*α *can1*Δ*::STE2pr-Sp_his5 lyp1*Δ*::STE3pr-LEU2 his3*Δ*1 leu2*Δ*0 ura3*Δ*0 flc1*Δ*::caURA3MX4 flc2*Δ*::NatMX4*	This study
*flc1*Δ *flc3*Δ	*MAT*α *can1*Δ*::STE2pr-Sp_his5 lyp1*Δ*::STE3pr-LEU2 his3*Δ*1 leu2*Δ*0 ura3*Δ*0 flc1*Δ*::caURA3MX4 flc3*Δ*::KanMX4*	This study
*flc1*Δ *yor365c*Δ	*MAT*α *can1*Δ*::STE2pr-Sp_his5 lyp1*Δ*::STE3pr-LEU2 his3*Δ*1 leu2*Δ*0 ura3*Δ*0 flc1*Δ*::caURA3MX4 yor365c*Δ*::HisMX4*	This study
*flc2*Δ *flc3*Δ	*MAT*α *can1*Δ*::STE2pr-Sp_his5 lyp1*Δ*::STE3pr-LEU2 his3*Δ*1 leu2*Δ*0 ura3*Δ*0 flc2*Δ*::NatMX4 flc3*Δ*::KanMX4*	This study
*flc2*Δ *yor365c*Δ	*MAT*α *can1*Δ*::STE2pr-Sp_his5 lyp1*Δ*::STE3pr-LEU2 his3*Δ*1 leu2*Δ*0 ura3*Δ*0 flc2*Δ*::NatMX4 yor365c*Δ*::HisMX4*	This study
*flc3*Δ *yor365c*Δ	*MAT*a *his3Δ1 leu2Δ0 met15Δ0 ura3Δ0 flc3*Δ*::KanMX4 yor365c*Δ*::HisMX4*	This study
*flc1*Δ *flc2*Δ *tetO-FLC3*	*MAT*α *can1*Δ*::STE2pr-Sp_his5 lyp1*Δ*::STE3pr-LEU2 his3*Δ*1 leu2*Δ*0 ura3*Δ*0 flc1*Δ*::caURA3MX4 flc2*Δ*::NatMX4 tetO2-FLC3-KanMX4*	This study
*flc1*Δ *flc2*Δ *yor365c*Δ	*MAT*α *can1*Δ*::STE2pr-Sp_his5 lyp1*Δ*::STE3pr-LEU2 his3*Δ*1 leu2*Δ*0 ura3*Δ*0 flc1*Δ*::caURA3MX4 flc2*Δ*::NatMX4 yor365c*Δ*::HisMX4*	This study
*flc1*Δ *flc3*Δ *yor365c*Δ	*MAT*α *can1*Δ*::STE2pr-Sp_his5 lyp1*Δ*::STE3pr-LEU2 his3*Δ*1 leu2*Δ*0 ura3*Δ*0 flc1*Δ*::caURA3MX4 flc3*Δ*::KanMX4 yor365c*Δ*::HisMX4*	This study
*flc2*Δ *flc3*Δ *yor365c*Δ	*MAT*α *can1*Δ*::STE2pr-Sp_his5 lyp1*Δ*::STE3pr-LEU2 his3*Δ*1 leu2*Δ*0 ura3*Δ*0 flc2*Δ*::NatMX4 flc3*Δ*::KanMX4 yor365c*Δ*::HisMX4*	This study

*flc1*Δ *flc2*Δ *tetO-FLC3 yor365c*Δ 1Δ2Δ3tyΔ	*MAT*α *can1*Δ*::STE2pr-Sp_his5 lyp1*Δ*::STE3pr-LEU2 his3*Δ*1 leu2*Δ*0 ura3*Δ*0 flc1*Δ*::caURA3MX4 flc2*Δ*::NatMX4 tetO2-FLC3-KanMX4 yor365c*Δ*::HisMX4*	This study
chs2-DAmP	*MAT*a *his3Δ1 leu2Δ0 met15Δ0 ura3Δ0 chs2-DAmP-KanMX4*	[1]
*bst1*Δ	*MAT*α *can1*Δ*::STE2pr-Sp_his5 lyp1*Δ*::STE3pr-LEU2 his3*Δ*1 leu2*Δ*0 ura3*Δ*0 bst1*Δ*::caURA3MX4*	This study
*per1*Δ	*MAT*α *can1*Δ*::STE2pr-Sp_his5 lyp1*Δ*::STE3pr-LEU2 his3*Δ*1 leu2*Δ*0 ura3*Δ*0 per1*Δ*::caURA3MX4*	This study
*gup1*Δ	*MAT*α *can1*Δ*::STE2pr-Sp_his5 lyp1*Δ*::STE3pr-LEU2 his3*Δ*1 leu2*Δ*0 ura3*Δ*0 gup1*Δ*::caURA3MX4*	This study
*cwh43*Δ	*MAT*α *can1*Δ*::STE2pr-Sp_his5 lyp1*Δ*::STE3pr-LEU2 his3*Δ*1 leu2*Δ*0 ura3*Δ*0 cwh43*Δ*::caURA3MX4*	This study
*gup1*Δ *cwh43*Δ	*MAT*α *can1*Δ*::STE2pr-Sp_his5 lyp1*Δ*::STE3pr-LEU2 his3*Δ*1 leu2*Δ*0 ura3*Δ*0 cwh43*Δ*::caURA3MX4 gup1*Δ*::KanMX4*	This study

Plasmids

Name	Type and markers	Source
pAG60	caURA3MX4	[3]

Primers for PCR

Number	Purpose	Sequence (5’-3’)
1388	Forward primer to swap KanMX4 to caURA3MX4	ACATGGAGGCCCAGAATACCC
1389	Reverse primer to swap KanMX4 to caURA3MX4	CAGTATAGCGACCAGCATTCAC

Materials and methods

Strains and reagents. Strains, plasmids and primers used are listed above. Cells were grown at 30°C on either YPD (1% yeast extract, 2% peptone, 2% glucose) or on synthetic complete (SC) medium (Yeast nitrogen base with (YNB) or without ammonium sulfate (YNB - A.S.)) plus dropout mix (amino acids, inositol, etc.) plus 2% glucose and plus 0.1% L-glutamic acid, when ammonium sulfate was omitted. Media for robotically crossing strains were the ones described in [4]. Sorbitol, glucose, G418, and Canavanine were from ForMedium (UK). Amino acids, Doxycycline, Thialysine, Chitinase from *Trichoderma viride*, Acyl-Coenzyme A synthetase from *Pseudomonas sp.,* Glycerol-3-phosphate, DTNB, Calcofluor white, Caspofungin diacetate, Tunicamycin from a *streptomyces* species, Triton TX-100, Digitonin, inositol, NaN_3, NaF and buffer salts were from Sigma. Coenzyme A (=CoA) trilithium salt was from Merck. [^{3}H]-*myo*-inositol, [^{3}H]-palmitic acid and [^{14}C]-Glycerol-3-phosphate were from ANAWA Trading SA (Switzerland). [^{3}H]-palmitoyl-CoA was synthesized as previously described [5]. Cerulenin was from Enzo Life Science AG (Switzerland), Zymolyase-20T from Seikagaku (Japan).

Preparation of strains for E-MAP Analysis. A list of 758 genes coding for proteins with two or more transmembrane regions, as predicted by the TMHMM algorithm, was obtained from the Comprehensive Yeast Genome Database (CYGD) (http://mips.helmholtz-muenchen.de/genre/proj/yeast/) (S6 Table). Of this list 579 deletion mutants were present in our EUROSCARF deletion library and 48 in our DAmP strain collection harboring hypomorphic alleles of essential genes [1]. *Ybr219c*Δ and *slc1*Δ were also included in our E-MAP strain collection. These 629 strains were grown in 200 µg/ml G418 at 24°C and frozen in 96-well plates containing liquid YPD supplemented with 15% glycerol. In the following, "query strains" designate strains harboring the two "magic markers" *can1*Δ*::STE2pr-Sp_his5* and *lyp1*Δ*::STE3pr-LEU2* plus a *xxxX::caURA3MX4* deletion; "array strains" designate *CAN1 LYP1 yyyY::kanMX* strains [6,7]. To obtain such query strains, we used the *MAT***a** array library from EUROSCARF and replaced the kanMX4 marker by the *caURA3MX4* marker containing the *URA3* of *Candida albicans* [3]. The swapping element was PCR amplified from the plasmid pAG60 with primers n°1388 and n°1389 and used to transform the array collection in microtiter plates with the LiAc/SS carrier DNA/PEG method as previously described [8]. After three consecutive rounds of transformations finally all the

mutants had become uracil prototroph and were streaked on agar plates; then single colonies were re-streaked in parallel on SC without uracil and YPD with G418. 590 of 629 mutants had lost G418 resistance and gained uracil prototrophy. The 590 uracil prototroph *MAT*a strains were mated with strain y8205 containing the magic markers, sporulated and *MAT*α or *MAT*a haploid progeny containing *can1*Δ*::STE2pr-Sp_his5 lyp1*Δ*::STE3pr-LEU2* plus a *xxxX::caURA3MX4* deletion was selected, thus creating the query strain set. 583 strains were obtained once in the *MAT***a** and once in the *MAT*α background. The two query sets were streaked again on agar plates, single colonies were randomly chosen and used to inoculate liquid YPD containing plates in 96-well format to be frozen at -80°C with 15% glycerol until use for E-MAPs.

To control for correct gene deletions, *MAT*a queries were robotically mated with the identical gene mutations in kanMX format, but coming from a different EUROSCARF deletion library than the one used to generate the query strains. After sporulation and selection of haploid double mutants, only few strains grew at the last selection. Growth suggested a false gene deletion; parents of growing strains were therefore controlled by PCR, replaced if necessary and controlled again by PCR. Thus, two sets of query strains, one *MAT*a and one *MAT*α, each containing 539 deletion and 44 hypomorphic mutants (DAmP), were thus prepared.

E-MAP Analysis

The genetic screen was done exactly as previously described [4], except that the *MAT*α query strains contained the *caURA3MX4* instead of *NATMX4* marker, the single mutant selection plates were replicated in parallel onto normal double mutant selection plates and on the same but supplemented with 0.4 µg/ml Cerulenin; these double mutant selection plates were incubated at 30°C for 24 h before pictures of the plates were taken. Cerulenin was titrated by robotically replicating the E-MAP *xxx::kanMX* array collection on plates with different concentrations of Cerulenin. As judged by visual inspection of plates, at concentrations of 0.4 µg/ml, most strains were still growing normally (S13 Fig). For the MSP-E-MAPs we used an array of 629 mutants in duplicates arranged horizontally with a maximal density of 1536 colonies per plate. Each one of the 583 queries was crossed with such an array plate. Color pictures were taken using a Nikon D90 (12.3 megapixels), focal length = 105 mm, F-number = 8, ISO = 200, mounted in a KAISER camera stand with two fixed TC-L lamps (36W). The plates were put on top of a black surface to have a uniform black background.

Plate pictures were cropped using Photoshop, treated with the HT Colony Grid Analyzer program and the resulting files processed using the E-MAP toolbox. All these software are described in [4,9] and can be downloaded from the web. The settings in the E-MAP toolbox for the processing of data were *2nd order surface* for position artifacts, *Parzen estimates* for normalization and control size estimations, *0.4* as threshold for removing frequently missing strains, *10* and *1000*, respectively, for minimum and maximum size threshold.

All P-values used for the selection of significance thresholds were calculated separately for negative and positive values throughout and were computed using the (one tailed) probability density calculation of the Excel NORM.DIST function. Unless indicated otherwise, P values were not adjusted, e.g. by Bonferroni or Benjamini-Hochberg corrections. Thus, we considered as significant those genetic interactions having unadjusted P-values of <0.005, correlations having P-values <0.05, because these significance levels appeared to be similar to the thresholds used in other E-MAP studies. Indeed, Bonferroni correction removed many interactions and corrections that made biological sense. E.g. the clear dependence between correlations and mean S scores of Fig 2 would be between non-significant correlations and S scores. Significance levels based on Bonferroni-corrected P values (P<0.05) are however indicated by dotted lines in Fig 2 and interactions and correlations being signficant under these more stringent criteria are marked in S2B Table.

Data clean up

As shown in S6 Table, from a total of 629 strains present in the array and 583 strains present in the queries, 17 and 16 strains, respectively, were eliminated because of their proximity to *CAN1* or *LYP1* (< 100 kbp up or downstream) 10 and 21 strains, respectively, were eliminated due to mating, sporulation or germination problems, 42 mutants were eliminated in both queries and arrays because in systematic visual inspection of the plates they were considered to be noisy, showed very inconstant scoring or colony sizes and counted more than 10 interactions with an S score difference $\geq |5|$ between the unaveraged S scores of the reciprocal [query A x array B] and [query B x array A] crosses. Additionally, 17 mutants were eliminated from the array setup due to very slow growth. The final E-MAPs contained 146'412 genetic interactions and interaction profile correlations. In addition, some genetic interactions were eliminated by the software for different reasons (gene proximity, missing colonies, etc.) resulting in the final MSP- and MSP/C-E-MAPs containing the 142,108 and 142'114 validated genetic interactions listed in S2A Table. After cleaning, the final array set

contained 543 strains and the final query set 504 strains (S6 Table). Thus, the final MSP-E-MAP scores were calculated from validated 504 reciprocal and 39 one way crosses (S2 Table). Strains were always eliminated from both datasets obtained without and with Cerulenin. Removal of noisy strains indeed increased the correlation between reciprocal crosses (S1A Fig - S1D Fig) and removed almost many genetic interactions located along the x- and y-axis in S1A Fig, to yield the validated interactions of non-noisy strains shown in S1B Fig. Some non-noisy strains still gave different values in reciprocal crosses, mainly the ones showing positive S scores on Cerulenin (Fig 1E, S1D Fig); for such strains the final S scores listed in S2A, S4 and S3 Tables and reported as heat map in S8 Fig always contained the averaged S scores comprising the values of the two (uneven) reciprocal crosses. The final dataset is reported by 543 x 543 heat maps and matrices (S8 Fig; S4 and S3 Table). Of the [(543 x 543) - 543]/2 =147'153 theoretical combinations of two different genes in such a matrix, [(39 x 39) - 39]/2 = 741 were not tested, and 504 x 39 = 19'656 were tested only in one way, whereas [(504 x 504) - 504]/2 = 126'756 were tested by reciprocal crosses. 84 randomly chosen queries were crossed with the array in a repeat experiment, generating again [(84 x 84) - 84]/2 = 3486 reciprocal crosses, and 38556 one directional crosses. These repeat data were also integrated into the final data reported in S2, S4, and S3 Tables and S8 Fig, which thus show the average of all data obtained for each given gene combination. Significant genetic interactions were generated by 528 of the 543 genes of the E-MAP set (S2B Table).

Hierarchical clustering

For S8 Fig, the matrix containing all correlations (S4B Table) was subjected to hierarchical clustering, thus generating a “correlation of correlations matrix”, i.e. juxtaposing genes having the same profile of correlations and resulting in the matrix of S3B Table. The corresponding heat map is in S8B. Substituting genetic interaction scores into the same hierarchical clustering canvas using the matrix of S3A Table generated S8A Fig. When the matrix of genetic interactions (S4A Table) was used as a base of the hierarchical clustering process, i.e. when data were clustered based on the genetic interaction profiles, we obtained a very similar heat map, containing all the clusters and boxes of S8 Fig, although genes were in slightly different order. For the visualization of the data in heat maps, data from the final E-MAP toolbox file were first clustered using the Cluster 3.0 program then visualized using the Java Treeview program. Both of these software can be downloaded at http://bonsai.hgc.jp/~mdehoon/software/cluster/software.htm#ctv.

153

154 *Microsome preparation*

155 Cells grown during 16 h to an OD_{600} of 1 - 2 in YPD + 1.4 M sorbitol in the absence or
156 presence of 10 µg/ml Doxy, were centrifuged and resuspended in zymolyase buffer (10 mM
157 NaN_3, 1.4 M sorbitol, 50 mM potassium phosphate pH 7.5, 40 mM β-mercaptoethanol, 1 mg
158 ml^{-1} zymolyase 20T) followed by an incubation of 1 h at 30°C without shaking. Spheroplasts
159 were collected by centrifugation at 800 x g for 5 min at 4 °C and washed with one volume of
160 zymolyase buffer lacking β-mercaptoethanol and zymolyase. Spheroplasts were lysed in lysis
161 buffer (1.4 M sorbitol, 3 mM $MgCl_2$, 50 mM potassium phosphate pH 7.5, 5 µg ml^{-1}
162 pepstatin A and 1 x EDTA-free Roche protease inhibitor cocktail) by forcing them 20 times
163 through a 0.4 mm gauge needle. After centrifugation at 1000 x g for 5 min at 4 °C, the
164 supernatant was centrifuged at 16000 x g for 60 min at 4 °C to pellet the microsomes. The
165 supernatant was discarded and microsomes were resuspended in small volumes of lysis
166 buffer lacking protease inhibitors.

167

168 *Metabolic radiolabeling of cells and microsomes*

169 For the labeling of lipids with [^{3}H]-C16:0 (Fig 4A - 4C), 10 OD_{600} of WT or 1Δ2Δ3tyΔ cells
170 grown with or without 10 µg/ml Doxy for the indicated times in YPD or YPD + 1.4 M
171 sorbitol, were centrifuged and resuspended in 2 ml SC medium supplemented with 10 µg/ml
172 Cerulenin and preincubated for 20 minutes at 30°C. Twenty µCi (≅ 0.3 µM) [^{3}H]-C16:0 were
173 then added and the cultures incubated at 30°C for the indicated time periods. The lipids of all
174 assayed cells were extracted, treated with NaOH if indicated, spotted and separated by TLC
175 with solvent 1. Labeling of lipids with [^{3}H]-*myo*-inositol (Fig 4D) was done by growing cells
176 in inositol-free SC medium containing 1.4 M sorbitol and supplemented or not with 10 µg/ml
177 Doxycycline for 16 hours. Aliquots of 10 OD_{600} units of cells were collected, centrifuged and
178 resuspended in 1 ml fresh medium of the same kind, 40 µCi of [^{3}H]-*myo*-inositol were added
179 (t = 0) and the cells were put back to 30°C without cover for good aeration. Fresh medium
180 (0.2 ml) from a 5x concentrated stock was added at t = 40 and 80 min. Labeling was stopped
181 after 2 h. Lipids of 10 OD_{600} units of cells were extracted, spotted and separated by TLC with
182 solvent 2.

183 For labeling of lipids in microsomes (Fig 5), 50 µg of microsomal protein were incubated at
184 room temperature for the indicated times in 1.4 M sorbitol, 3 mM $MgCl_2$, 50 mM potassium
185 phosphate pH 7.5 with 6.6 µM (0.1 µCi) [^{14}C]-G3P and the indicated concentrations of

C16:0-CoA and Triton X-100 in a final volume of 100 µl. Lipids were extracted and separated by TLC with solvent 1. Labeling of GPI anchor lipids in cells (Fig 10C) and their isolation was done as previously described in [10] except that after washing, the elution of anchor peptides from octyl-Sepharose was done directly with 50% propanol and that twice the number of cells and double amounts of radioactivity were used to label *per1*Δ, *gup1*Δ and *gup1*Δ *cwh43*Δ mutants and that therefore, for these strains, doubled amounts of lipids were spotted on the TLC shown in Fig 10C. Anchor lipids were resolved on TLC in solvent 3. The microsomal labeling of GPI lipids (Fig 8), was done as previously described in [11] but with the following modifications: 100 µg of microsomal protein in a final volume of 100 µl were incubated at room temperature for the indicated times in buffer (1.4 M sorbitol, 50 mM potassium phosphate pH 7.5, 3 mM $MgCl_2$, 0.5 mM $MnCl_2$, 1 mM EGTA) supplemented with 1 mM Coenzyme A, 1 mM ATP and 21 µg/ml Tunicamycin except in one control where ATP and CoA were omitted and 1 mM Glycerol-3-phosphate was added.

Metabolic radiolabeling of permeabilized cells

Cells were grown for 16 h in YPD + 1.4 M sorbitol with or without 10 µg/ml Doxy and washed with buffer (50 mM potassium phosphate pH 7.5, 1.4 M sorbitol, 10 mM NaN_3, 3 mM $MgCl_2$). Cells were resuspended at an OD_{600} of 10 in the same buffer and aliquots of 1 ml were supplemented with different concentrations of Digitonin as indicated. Then the 1 ml aliquots were preincubated during 30 minutes at room temperature to allow the permeabilization of the plasma membrane. The acyltransferase activities of cells were assayed at room temperature by adding either C16:0-CoA (10 µM final) and [^{14}C]-G3P (0.5 µCi, 10 µM final)(Fig 6 and S5 Fig), or [^{3}H]-C16:0-CoA (1 µCi, 10 µM final) and other ingredients as indicated (Fig 7). Lipids were extracted and separated by TLC with solvent 1.

Lipid extraction from cells and microsomes

Lipids were extracted from cell pellets by first mechanically disrupting the cells with glass beads in chloroform-methanol (2:1), the lysate was then centrifuged and the pellet further extracted with 95% ethanol-water-diethyl ether-pyridine-4.2 N ammonium hydroxide (15:15:5:1:0.18). The supernatants containing the lipids were pooled, dried and desalted by butanol-water partitioning as described [10]. When microsomes were assayed, butanol was used to stop the reactions and extract the lipids. To extract radiolabeled GPI lipid intermediates from microsomes (Fig 8), 667 µl chloroform-methanol (1:1) was added

yielding a final ratio of chloroform-methanol-water of 10:10:3 and the tubes were vigorously vortexed. The tubes were centrifuged at 10'000 g for 5 minutes and the supernatant transferred to a separate tube. The pellet was extracted once more with chloroform-methanol-water (10:10:3) and the pooled supernatants were dried. The dried lipids were desalted by butanol–water partitioning as described by [10], dried again, resuspended and separated on TLC using solvent 4.

Lipid analysis

Lipids were analyzed by TLC on silica gel 60 glass plates. The solvents used in this study were solvent 1 (chloroform-methanol-0.25% KCl, 55:45:5), solvent 2 (chloroform-methanol-2N ammonia, 9:7:2), solvent 3 (chloroform–methanol–0.25% KCl, 55:45:10) or solvent 4 (chloroform–methanol–water, 10:10:3). For Fig 7, PI was distinguished from PA by scraping the silica from TLC plates (except for origin), extracting the silica with solvent 4 and treating the dried extract in NEBuffer 3™ (New England Biolabs) supplemented with 0.1% deoxycholate with or without 50 U alkaline phosphatase (AP) at 37°C for 2 h. The lipids were extracted twice from the aqueous solution by adding chloroform-methanol (2:1), the organic phases were pooled and dried, resuspended in solvent 4, spotted and separated again by TLC with solvent 1. For mild base treatment, dried lipids were resuspended in 200 μl chloroform–methanol– water (10:10:3), 40 μl of 0.6 M NaOH in methanol was added, and samples were incubated at 37°C for 1 h. Hydrolysis was stopped with 40 μl of 0.8 M acetic acid, and the lipids were dried. Control samples followed the same procedure, but NaOH and acetic acid were added together at the end of the incubation. Dried lipids were desalted by butanol–water partitioning as described by [10].

Supplemental Figure legends

S1 Fig. Processing of raw E-MAP data. (A - D) S scores of double mutants observed on [query A x array B] plates vs. S scores of same double mutants observed on [query B x array A] plates are plotted. For this, for each gene combination, the software averages the size of the two colonies on the [query A x array B] and on the [query B x array A] plate separately and thereby generates a so-called unaveraged score for each [9]. Thus, the x- and y-coordinates of each dot indicate these unaveraged S scores obtained in the two reciprocal crosses ([*aaaA::ura3MX* x *bbbB::kanMX*] and [*bbbB::ura3MX* x *aaaA::kanMX*]). (Crosses done only in one direction are not plotted). (A, B) S scores of MSP-E-MAP before (A) and after (B) removal of noisy strains. (C, D) S scores in MSP/C-E-MAP before (C) and after (D) removal of noisy strains. Panels (B) and (D) correspond to Fig 1D and 1E and are shown here once more to demonstrate that elimination of noisy strains increases the correlation between unaveraged S scores obtained in reciprocal crosses. (E, F) the similarity between reciprocal crosses can also be seen when calculating medians of the second unaveraged S scores as a function of first unaveraged score using the software of [9,12]. The plot was calculated after having removed noisy strains. (E) MSP-E-MAP; (F) MSP/C-E-MAP. The not quite proportional lines in (E) and (F) are very similar to the ones obtained in the ESP-E-MAP, i.e. Figure S1 of [12] and Fig 3b of [9]. (G, H) with the data of Fig 2, the ratio of the numbers of gene pairs giving significantly positive over significantly negative S scores was calculated as a function of the correlation for the MSP-E-MAP (G) and the MSP/C-E-MAP (H) using a window of 30 values.

S2 Fig. Reproducibility of correlations of the MSP-E-MAP and MSP/C-E-MAP. (A, B) a subset of 84 queries were crossed once more with the 629 genes of the array without (A) or with Cerulenin (B) by different persons (authors Christine Vionnet and Carole Roubaty) and the interaction profile correlations compared to those obtained in the first MSP- and MSP/C-E-MAP (carried out by author Hector M. Vazquez) as described in Fig 1F, 1G legend. The trend lines and the corresponding Pearson correlation values of the two replications are for all the correlation coefficients (black) or only statistically significant correlations (blue). The dashed line represents a correlation of R = 1.

S3 Fig. Division times of single or combined *flc* mutants. (A) WT, single or multiple *flc* mutants (labeled as in Fig 3A) were inoculated in 200 µl YPD containing or not 0.1, 1 or 10

µg/ml Doxycycline and their growth rates were measured using an automated Bioscreen C MBR reader. Three independent strains were tested for each genotype. (B) mean division times were calculated from the exponential growth phase of curves of panel A.

S4 Fig. Permeabilization of cells with Digitonin and detection of cytosolic thiol groups with DTNB. WT or 1Δ2Δ3tyΔ cells grown for 16 h in YPD + 1.4 M sorbitol with (A, B) or without (C) 10 µg/ml Doxy were centrifuged and resuspended in buffer (50 mM potassium phosphate pH 7.5, 1.4 M sorbitol, 10 mM NaN_3, 3 mM $MgCl_2$) at an OD_{600} of 20. Then, 500 µl of the same buffer supplemented with 2 x the desired concentration of Digitonin plus 2 mM DTNB were mixed with 500 µl of the cell suspension and the absorbance was continuously measured at 412 nm at room temperature. The curves in the charts are the average of two independent biological replicates.
Interpretation: Intact cells are resuspended in the same buffer and at the same concentration as used for labeling permeabilized cells (Fig 6, S5 Fig), but with DTNB. The increase of absorbance in presence of cells (only cells, no detergent) is only slightly faster than the spontaneous hydrolysis of DTNB observed in the samples without cells (panels A, B), suggesting that the cells remain intact and that, as previously described, the DTNB cannot penetrate the plasma membrane [13,14]. When adding 0.001% or higher concentrations of Digitonin, the plasma membranes of WT and 1Δ2Δ3tyΔ cells begin to lyse and DTNB starts to react with the sulfhydryl groups, mainly of proteins which remain in the cytosol [13,14]. The speed of this reaction increases with the concentration of Digitonin. 1Δ2Δ3tyΔ cells grown in Doxy are rather more resistant to plasma membrane solubilization than WT cells (panel B vs. A), and also slightly more resistant than 1Δ2Δ3tyΔ cells grown without Doxy (panel B vs. C). 1Δ2Δ3tyΔ cells seem to retain a full redox potential as the reaction reaches plateau at similar values as in WT and since at high concentrations of Digitonin (0.02%) the reaction rate is the same for 1Δ2Δ3tyΔ cells and WT.

S5 Fig. 1Δ2Δ3tyΔ mutants have normal GPAT and AGPAT activity when not incubated with Doxy. (A, B) acyltransferase activity of WT and 1Δ2Δ3tyΔ cells was assayed with 10 µM C16:0-CoA and 10 µM [^{14}C]-G3P after preincubation in 0.001% (A) or 0.005% (B) Digitonin.

S6 Fig. Comparison of growth rates of *elo3*Δ, *cst26*Δ and *elo3*Δ *cst26*Δ cells. (A, B) exponentially growing cells were inoculated at an OD_{600} of 0.1 and grown in YPD at 30°C. OD_{600} values were measured at regular intervals. Four different *elo3*Δ *cst26*Δ strains derived from different spores generated by tetrad dissection were tested, two in (A), two in (B).

S7 Fig. Growth defects of mutants in the right arm of Chromosome II combined with *chs1*Δ. (A) growth of double mutants giving strong negative S scores (Fig 11A) was assayed in liquid culture using the Bioscreen C MBR reader allowing to calculate doubling times. The same medium as in the last selection step of the screen was used. The only double mutant having a significant difference with regard to corresponding single mutants is the unrelated *gup1*Δ *cwh43*Δ strain, which has an S score of - 9.9 and was added here as a positive control. (B) double mutants containing *chs1*Δ plus a deletion of some gene on the right arm of Chr. II together with corresponding parental single mutants were plated in four fold serial dilutions on the same medium as used in the last selection step of the MSP-E-MAP.

S8 Fig: Heat maps and main clusters of the MSP-E-MAP. Hierarchical clustering generated heat maps showing the genetic interaction S scores (A) and profile correlations (B) of the MSP-E-MAP. The main clusters are highlighted by circled numbers. Zones of frequent interactions or correlations outside the diagonal are either boxed or annotated at the right side of panel A by constituent gene names. In (A), gray dots indicate "no value" because gene combinations were not tested or values were eliminated for one of several reasons (see *Data clean up*). (C) enlarged views of the clusters placed into boxes in (A) and (B). Genes making up the clusters are indicated at the left in color code according to the functional categories attributed in S1 Table. The string of color codes is repeated at the top for easy reference. The interaction of the "microcluster" of *ELO3/SAC1* with genes of cluster 1 is shown to the right. Further enlargements of colored regions outside the diagonal showing a high density of interactions and/or correlations between clusters are shown in S9 Fig.

S9 Fig. Enlargement of regions in heat maps of S8A and S8B Fig showing frequent interactions or correlations between genes belonging to two different clusters. To the left, the clusters shown in S8C Fig are shown once more, spelling out the gene names making up each cluster in color code mode to indicate their functional category (S1 Table). More to the right follow cluster intersections. In all cluster intersections the same zone is shown once from the correlation map (S8B Fig) and once from the interaction map (S8A Fig), side by

side. For instance, in the first row, the enlargements of the heat maps show interactions and correlations of genes of cluster 1 with genes of clusters 2, then 3, then 4, then 5 and finally, to the right, cluster 6. On top of each cluster intersection, the color codes of the intersecting cluster are repeated twice, once for the interaction map, once for the correlation map. Some zones with frequent interactions outside the cluster intersections are also shown and the names of the genes in those zones are indicated above the top row but are the same for all zones below. The figure highlights for instance the negative interactions and correlations between clusters 3 and 5 or the positive interactions between clusters 5 and 6, the positive interactions of *ilm1*Δ with cluster 6 and intriguing negative interactions of *sur1*Δ (=*csg1*Δ) with cluster 5 mentioned also in the text.

S10 Fig. Frequency of significant interactions and correlations within and amongst different functional classes of genes. (A) as introduced in S1 Table, each of the 543 genes of the E-MAP set was allocated to one of 11 functional categories represented by the color code on the left and repeated at the top and at the bottom. The number of genes present in each category is indicated at the far left. Each square gives the number of significant negative (upper, olive) or significant positive (lower, orange) S scores (below diagonal) or correlations (above diagonal), as a percentage of the total number of gene combinations possible between the category indicated at the left end of row and the category at the bottom or top of the column. For columns, the functional category is only indicated by repeating the color code used for rows. If interactions were randomly distributed one would expect for negative and positive interactions values of 0.4 and 0.6 %, for negative and positive correlations of 0.4 and 0.6 %, respectively. (B) the same as in (A) but for the MSP/C-E-MAP. Here, only those percentages, which underwent a significant change (P value ≤ 0.05) in comparison with the MSP-E-MAP are shown. In all panels, the intensity of olive and orange coloring of values is proportional to the percentage.

S11 Fig. Interdependence of the number of interactions and correlations generated by the MSP-E-MAP. (A) from the matrix of interaction scores of the MSP-E-MAP (S4A Table), the number of significant positive and significant negative genetic interactions was counted for each one of the 543 genes of the E-MAP set using the COUNTIF function in EXCEL as detailed in S6A Table. Each gene is represented by a dot with x and y coordinates indicating the number of its significant positive and its significant negative interactions,

respectively. The correlation coefficient R as well as the average number of positive and negative interactions is indicated. (B) is as (A), yet not the number of interactions, but rather the sum of the positive and of the negative S scores in all significant interactions was calculated for each gene as shown in S7B Table. (C) the number of positive correlations was plotted as a function of the number of negative interactions for each of the 543 genes. (D) is as (A), but the number of correlations rather than interactions was obtained from the 543 x 543 correlation matrix (S4B and S7A Table). (E) from the 543 x 543 matrix of interaction and correlation scores (S4A and S4B Table), we tabulated for each gene the number of significant negative and positive genetic interactions as well as of significant positive and negative correlations it had generated. Then, the 543 genes of the E-MAP set were placed into 4 classes depending on whether they showed no, only positive, only negative or both types of genetic interactions; independently they were categorized into 4 classes depending on the correlations they had generated. By combining the 4 interaction and 4 correlation classes, a matrix with 16 categories was generated and each gene of the 543 attributed to one of these categories. Only 120 genes generated everything, negative and positive interactions and negative and positive correlations. (F) the correlations between the numbers of positive and negative interactions and positive and negative correlations generated by the 543 genes in both the MSP- and the MSP/C-E-MAP were calculated (S7D Table) and grouped into a Table giving in each field the correlation between the categories at the left of the row and at the top of the column. The green color is proportional to the correlation coefficient.

S12 Fig~~ure:~~ Comparison of E-MAPs with or without Cerulenin. (A, B) In (A) the sides of the grey box indicate the significance thresholds of S scores of double mutants in the MSP- and MSP/C-E-MAPs as used in Fig 2. Similarly, in (B) the grey box gives the significance thresholds of profile correlations between any two genes according to Fig 2. Values that underwent a strong increase (P value ≤ 0.005 for interactions, ≤ 0.05 for correlations) in the MSP/C-E-MAP as compared to the MSP-E-MAP are in red, those that underwent a significant decrease are green. For instance, the red dots above the box in (B) designate gene pairs that were not correlated without Cerulenin, but positively correlated on Cerulenin. The trend lines and the corresponding Pearson correlation values for all dots are in black, those for dots outside the grey box in blue. The dashed line represents correlation of R = 1.

S13 Fig. Titration of Cerulenin to determine its optimal concentration for the MSP/C-E-MAP. The MSP-E-MAP array gene set was robotically replicated on plates containing 0, 0.4, 0.5 and 0.6 µg/ml Cerulenin and incubated for 24 h at 30°C before pictures were taken.

Supplemental References (used in here and figure legends of supplemental figures)

1. Breslow DK, Cameron DM, Collins SR, Schuldiner M, Stewart-Ornstein J, Newman HW, et al. A comprehensive strategy enabling high-resolution functional analysis of the yeast genome. Nat Meth. 2008;5: 711–718. doi:10.1038/nmeth.1234

2. Vazquez HM, Vionnet C, Roubaty C, Conzelmann A. Cdc1 removes the ethanolamine phosphate of the first mannose of GPI anchors and thereby facilitates the integration of GPI proteins into the yeast cell wall. Mol Biol Cell. American Society for Cell Biology; 2014;25: 3375–3388. doi:10.1091/mbc.E14-06-1033

3. Goldstein AL, Pan X, McCusker JH. Heterologous URA3MX cassettes for gene replacement in Saccharomyces cerevisiae. Yeast. 1999;15: 507–511. doi:10.1002/(SICI)1097-0061(199904)15:6<507::AID-YEA369>3.0.CO;2-P

4. Collins SR, Roguev A, Krogan NJ. Quantitative genetic interaction mapping using the E-MAP approach. Meth Enzymol. 2010;470: 205–231. doi:10.1016/S0076-6879(10)70009-4

5. Bavdek A, Vazquez HM, Conzelmann A. Enzyme-coupled assays for flip-flop of acyl-Coenzyme A in liposomes. Biochim Biophys Acta. 2015;1848: 2960–2966. doi:10.1016/j.bbamem.2015.08.020

6. Costanzo M, Baryshnikova A, Bellay J, Kim Y, Spear ED, Sevier CS, et al. The genetic landscape of a cell. Science. American Association for the Advancement of Science; 2010;327: 425–431. doi:10.1126/science.1180823

7. Baryshnikova A, Costanzo M, Dixon S, Vizeacoumar FJ, Myers CL, Andrews B, et al. Synthetic genetic array (SGA) analysis in Saccharomyces cerevisiae and Schizosaccharomyces pombe. Meth Enzymol. 2010;470: 145–179. doi:10.1016/S0076-6879(10)70007-0

8. Gietz RD, Schiestl RH. Microtiter plate transformation using the LiAc/SS carrier DNA/PEG method. Nat Protoc. 2007;2: 5–8. doi:10.1038/nprot.2007.16

9. Collins SR, Schuldiner M, Krogan NJ, Weissman JS. A strategy for extracting and analyzing large-scale quantitative epistatic interaction data. Genome Biol. 2006;7: R63. doi:10.1186/gb-2006-7-7-r63

10. Guillas I, Pfefferli M, Conzelmann A. Analysis of ceramides present in glycosylphosphatidylinositol anchored proteins of Saccharomyces cerevisiae.

448 Meth Enzymol. 2000;312: 506–515.

449 11. Canivenc-Gansel E, Imhof I, Reggiori F, Burda P, Conzelmann A, Benachour
450 A. GPI anchor biosynthesis in yeast: phosphoethanolamine is attached to the
451 alpha1,4-linked mannose of the complete precursor glycophospholipid.
452 Glycobiology. 1998;8: 761–770. doi:10.1093/glycob/8.8.761

453 12. Schuldiner M, Collins SR, Thompson NJ, Denic V, Bhamidipati A, Punna T, et
454 al. Exploration of the Function and Organization of the Yeast Early Secretory
455 Pathway through an Epistatic Miniarray Profile. Cell. 2005;123: 507–519.
456 doi:10.1016/j.cell.2005.08.031

457 13. Battaglia G, Ryan AJ, Tomas S. Polymeric vesicle permeability: a facile
458 chemical assay. Langmuir. 2006;22: 4910–4913. doi:10.1021/la060354p

459 14. Liu Q, Siloto RMP, Weselake RJ. Role of Cysteine Residues in Thiol
460 Modification of Acyl-CoA:Diacylglycerol Acyltransferase 2 from Yeast.
461 Biochemistry. 2010;49: 3237–3245. doi:10.1021/bi9020499

462

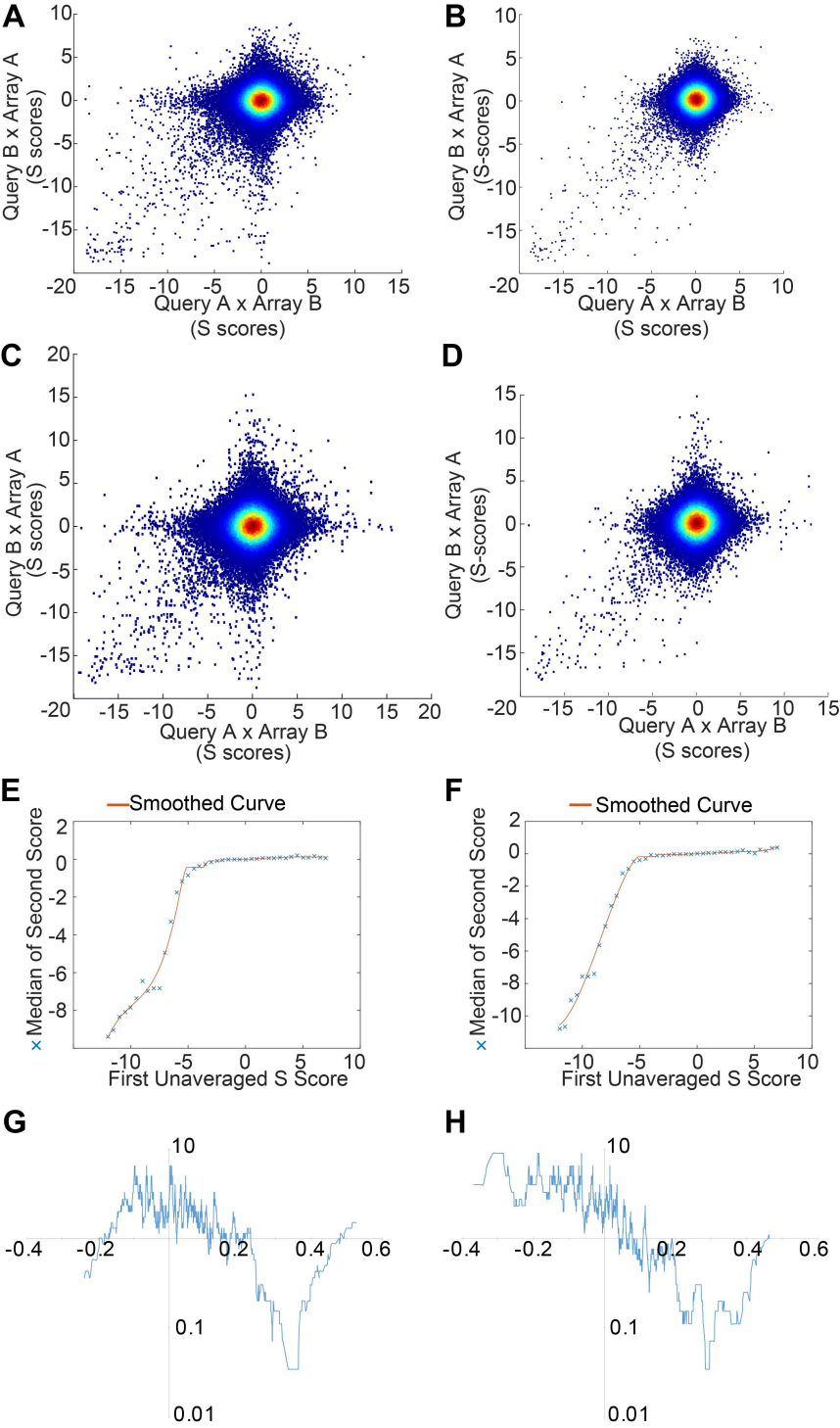
A
Query B x Array A
(S scores)
Query A x Array B
(S scores)
B
Query B x Array A
(S-scores)
Query A x Array B
(S scores)
C
Query B x Array A
(S scores)
Query A x Array B
(S scores)
D
Query B x Array A
(S-scores)
Query A x Array B
(S scores)
E
Smoothed Curve
Median of Second Score
First Unaveraged S Score
F
Smoothed Curve
Median of Second Score
First Unaveraged S Score
G
10
0.1
0.01
H
10
0.1
0.01

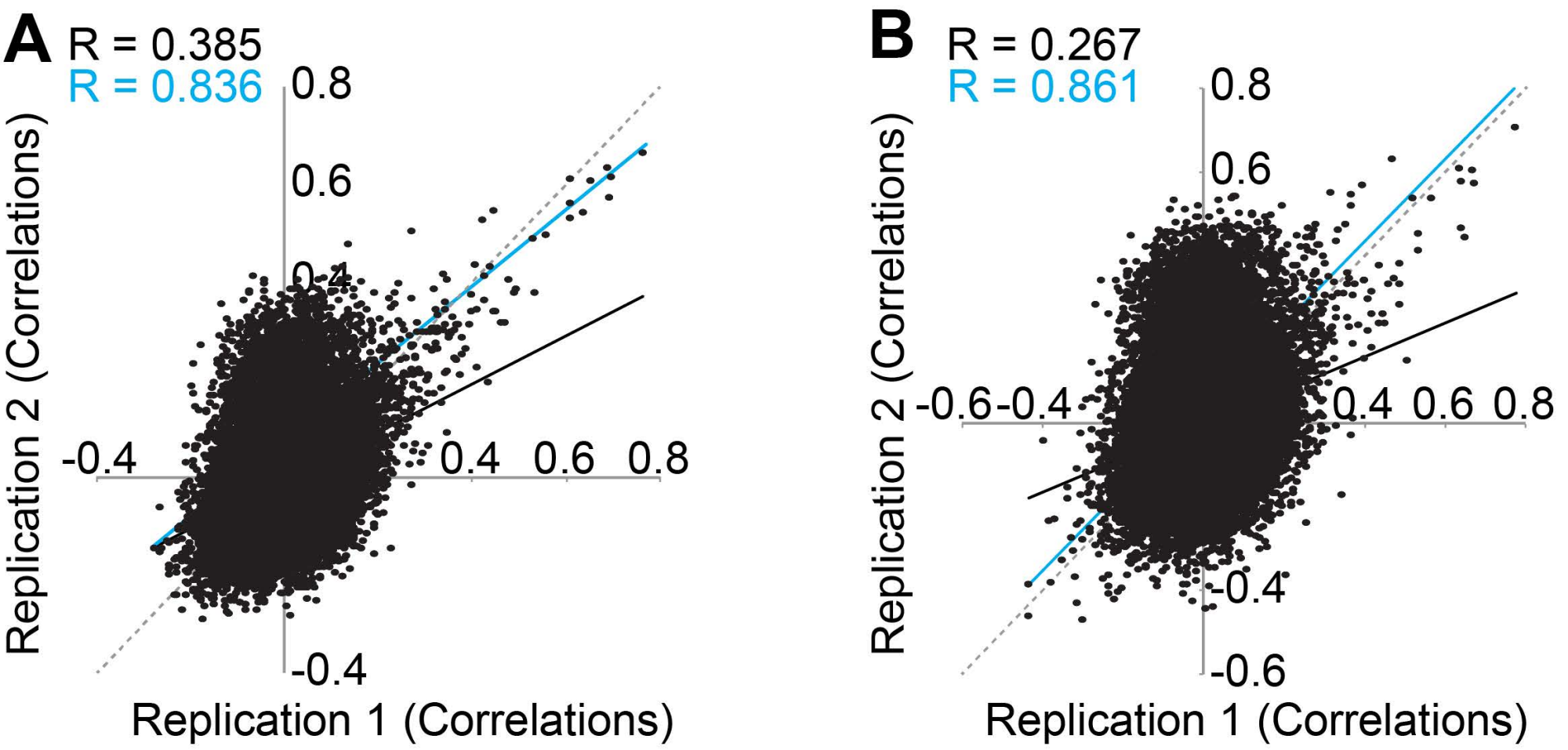
A
R = 0.385
R = 0.836
0.8
0.6
0.4
-0.4
-0.4
0.4
0.6
0.8
Replication 2 (Correlations)
Replication 1 (Correlations)
B
R = 0.267
R = 0.861
0.8
0.6
-0.6
-0.4
-0.6
-0.4
0.4
0.6
0.8
Replication 2 (Correlations)
Replication 1 (Correlations)

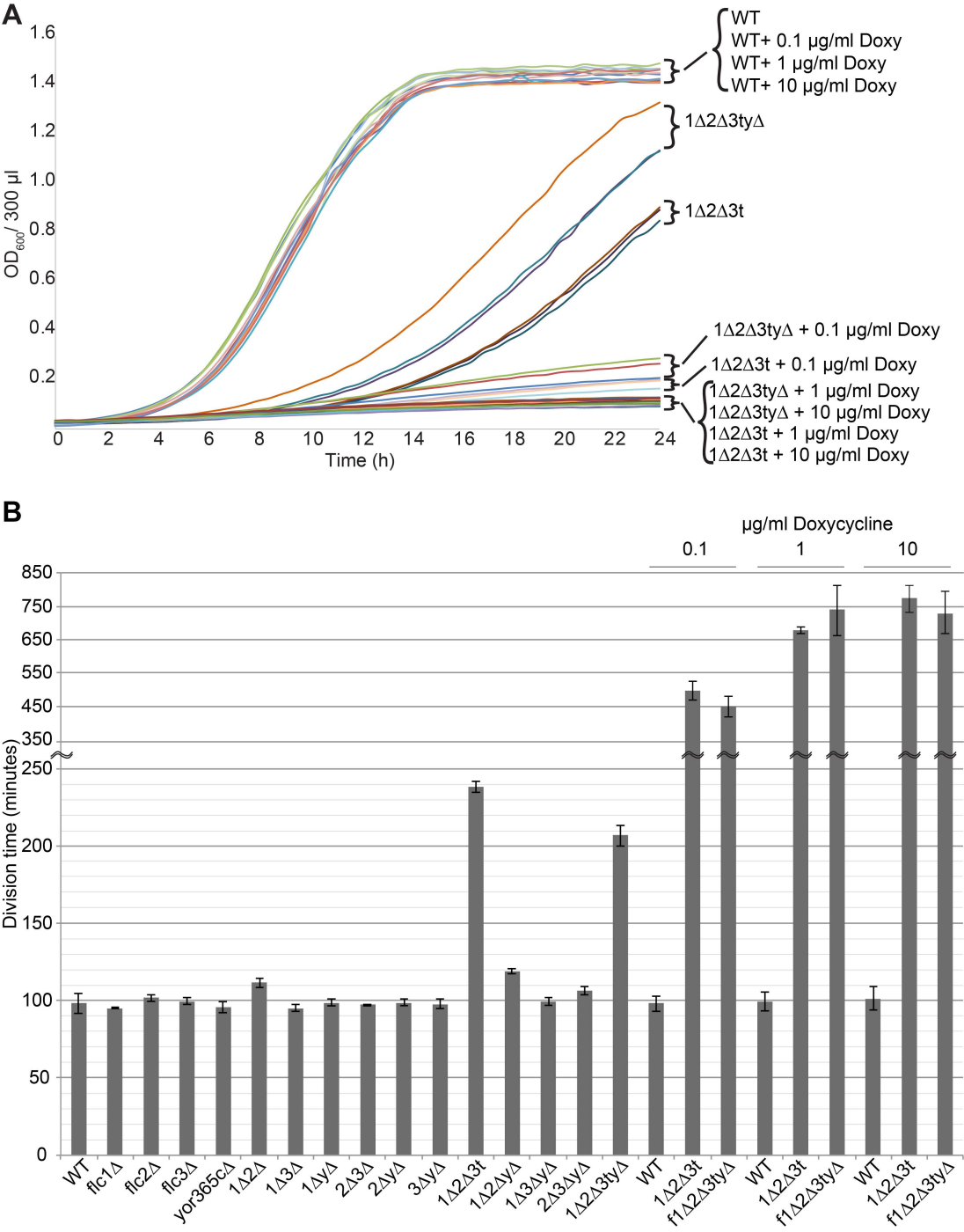
A
1.6
1.4
1.2
1.0
0.8
0.6
0.4
0.2
OD600/ 300 µl
0
2
4
6
8
10
12
14
16
18
20
22
24
Time (h)
WT
WT+ 0.1 µg/ml Doxy
WT+ 1 µg/ml Doxy
WT+ 10 µg/ml Doxy
1Δ2Δ3tyΔ
1Δ2Δ3t
1Δ2Δ3tyΔ + 0.1 µg/ml Doxy
1Δ2Δ3t + 0.1 µg/ml Doxy
1Δ2Δ3tyΔ + 1 µg/ml Doxy
1Δ2Δ3tyΔ + 10 µg/ml Doxy
1Δ2Δ3t + 1 µg/ml Doxy
1Δ2Δ3t + 10 µg/ml Doxy
B
µg/ml Doxycycline
0.1
1
10
Division time (minutes)
850
750
650
550
450
350
250
200
150
100
50
0
WT
flc1Δ
flc2Δ
flc3Δ
yor365cΔ
1Δ2Δ
1Δ3Δ
1Δyδ
2Δ3Δ
2Δyδ
3Δyδ
1Δ2Δ3t
1Δ2Δyδ
1Δ3Δyδ
2Δ3Δyδ
1Δ2Δ3tyΔ
WT
1Δ2Δ3t
f1Δ2Δ3tyΔ
WT
1Δ2Δ3t
f1Δ2Δ3tyΔ
WT
1Δ2Δ3t
f1Δ2Δ3tyΔ

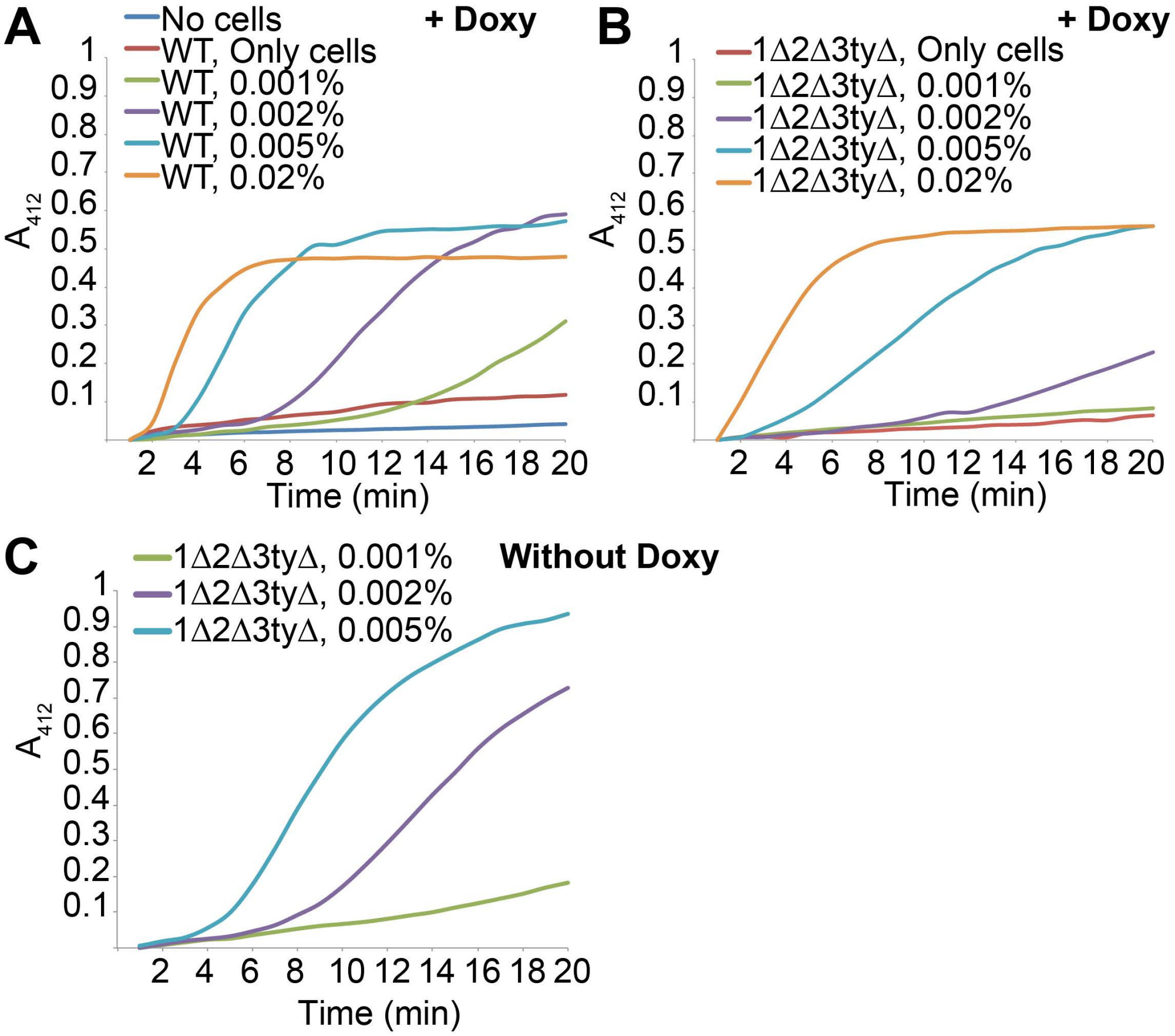
A
No cells
WT, Only cells
WT, 0.001%
WT, 0.002%
WT, 0.005%
WT, 0.02%
+ Doxy
A412
Time (min)
B
1Δ2Δ3tyΔ, Only cells
1Δ2Δ3tyΔ, 0.001%
1Δ2Δ3tyΔ, 0.002%
1Δ2Δ3tyΔ, 0.005%
1Δ2Δ3tyΔ, 0.02%
+ Doxy
A412
Time (min)
C
1Δ2Δ3tyΔ, 0.001%
1Δ2Δ3tyΔ, 0.002%
1Δ2Δ3tyΔ, 0.005%
Without Doxy
A412
Time (min)

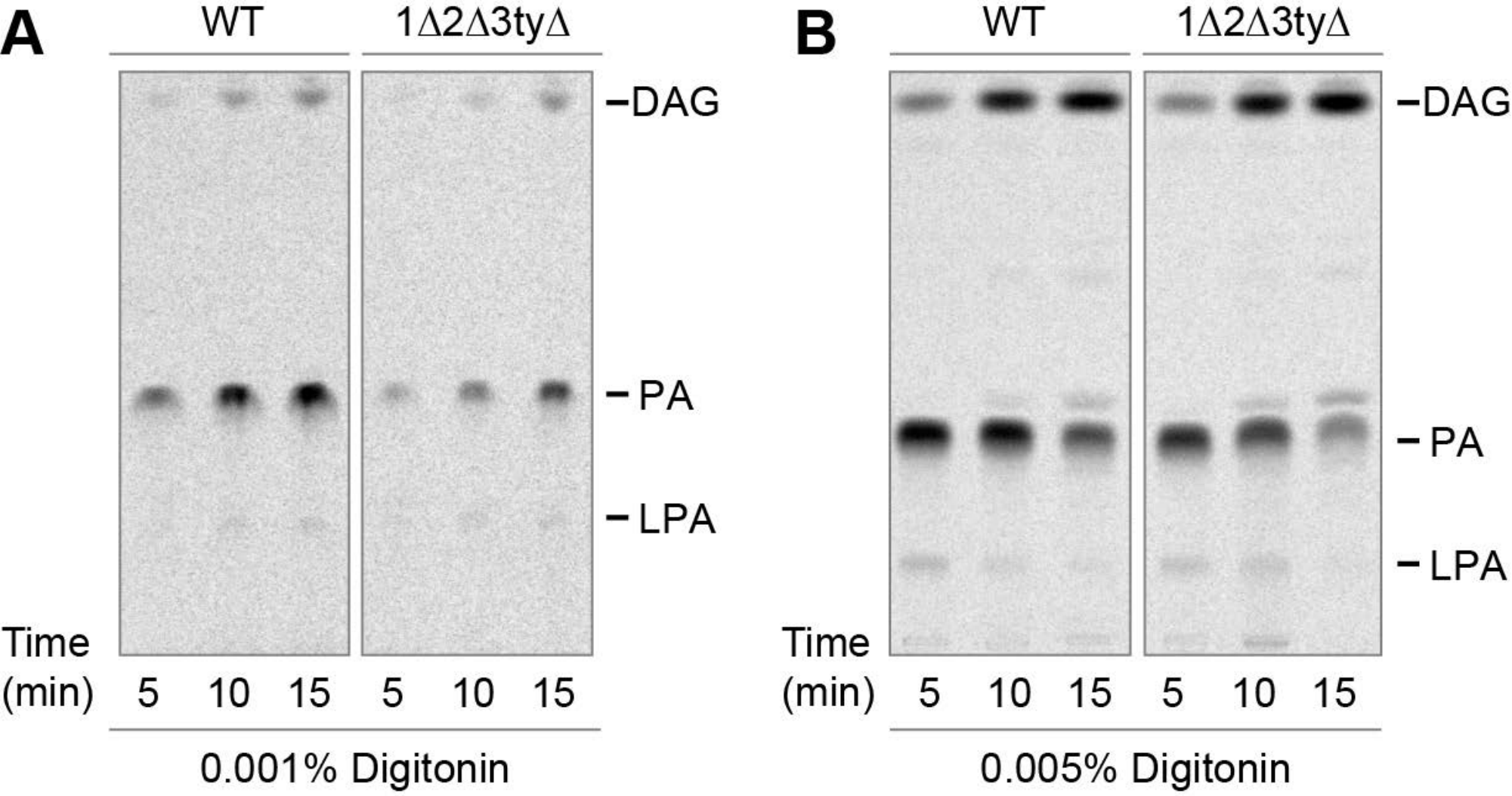
A
WT
1Δ2Δ3tyΔ
DAG
PA
LPA
Time
(min)
5
10
15
5
10
15
0.001% Digitonin
B
WT
1Δ2Δ3tyΔ
DAG
PA
LPA
Time
(min)
5
10
15
5
10
15
0.005% Digitonin

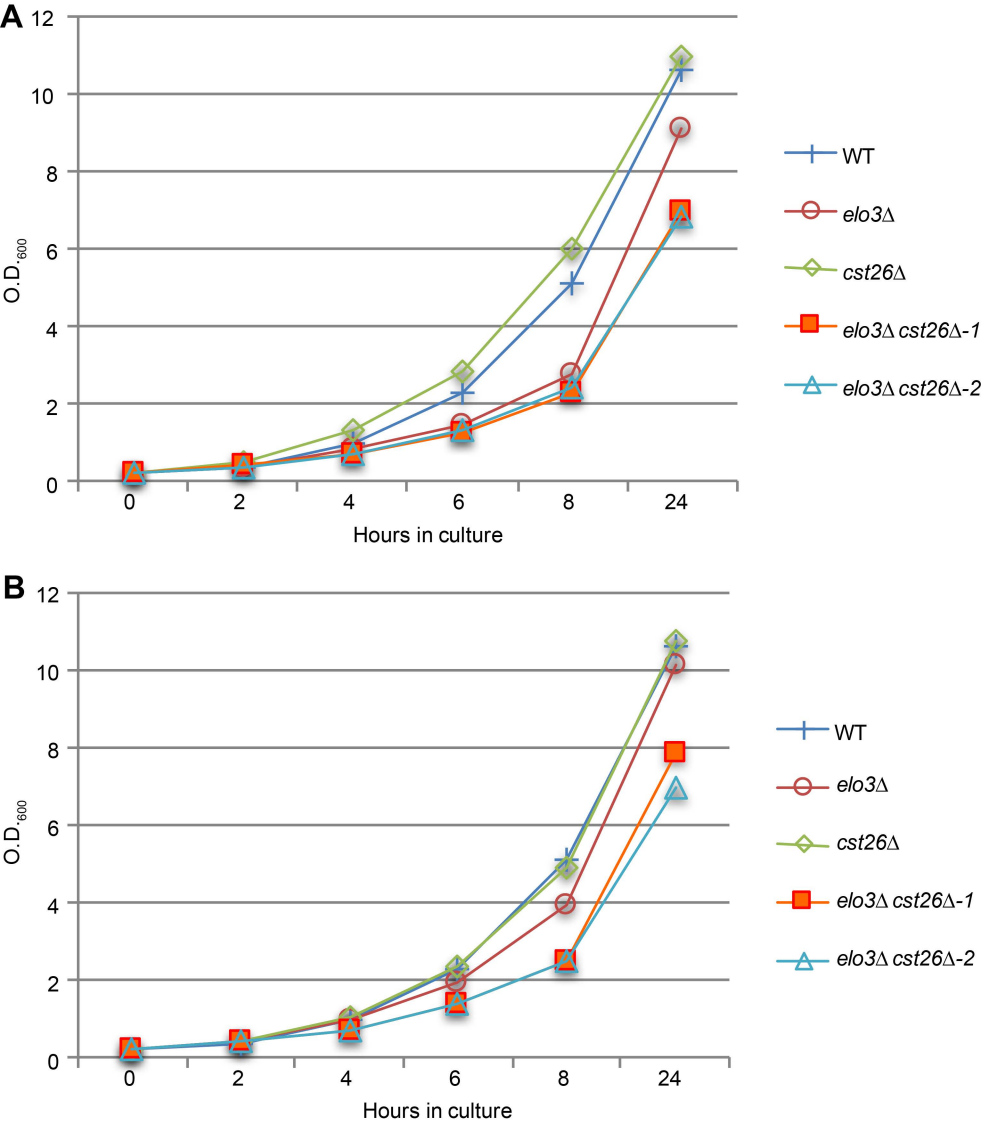
A
12
10
8
6
4
2
0
O.D.600
0
2
4
6
8
24
Hours in culture
WT
elo3Δ
cst26Δ
elo3Δ cst26Δ-1
elo3Δ cst26Δ-2
B
12
10
8
6
4
2
0
O.D.600
0
2
4
6
8
24
Hours in culture
WT
elo3Δ
cst26Δ
elo3Δ cst26Δ-1
elo3Δ cst26Δ-2

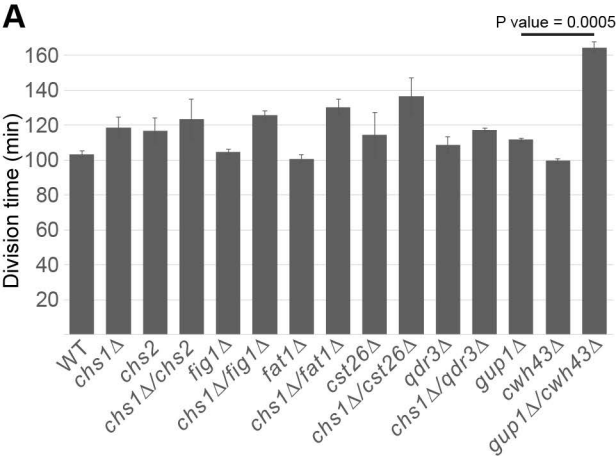
A
P value = 0.0005
Division time (min)
160
140
120
100
80
60
40
20
WT
chs1Δ
chs2
chs1Δ/chs2
fig1Δ
chs1Δ/fig1Δ
fat1Δ
chs1Δ/fat1Δ
cst26Δ
chs1Δ/cst26Δ
qdr3Δ
chs1Δ/qdr3Δ
gup1Δ
cwh43Δ
gup1Δ/cwh43Δ

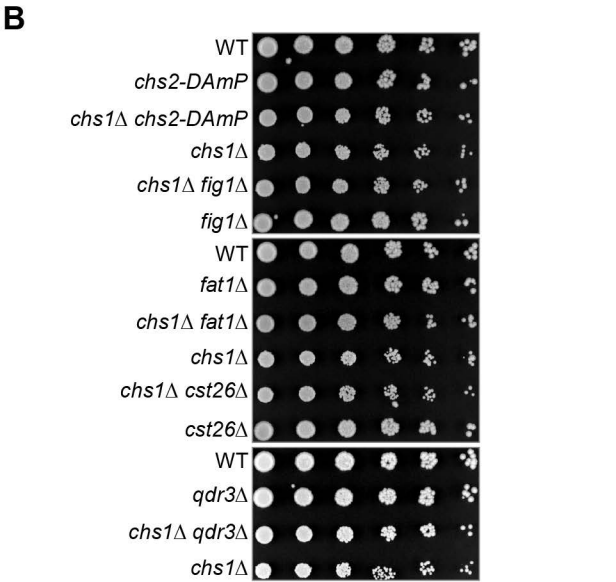
B
WT
chs2-DAmP
chs1Δ chs2-DAmP
chs1Δ
chs1Δ fig1Δ
fig1Δ
WT
fat1Δ
chs1Δ fat1Δ
chs1Δ
chs1Δ cst26Δ
cst26Δ
WT
qdr3Δ
chs1Δ qdr3Δ
chs1Δ

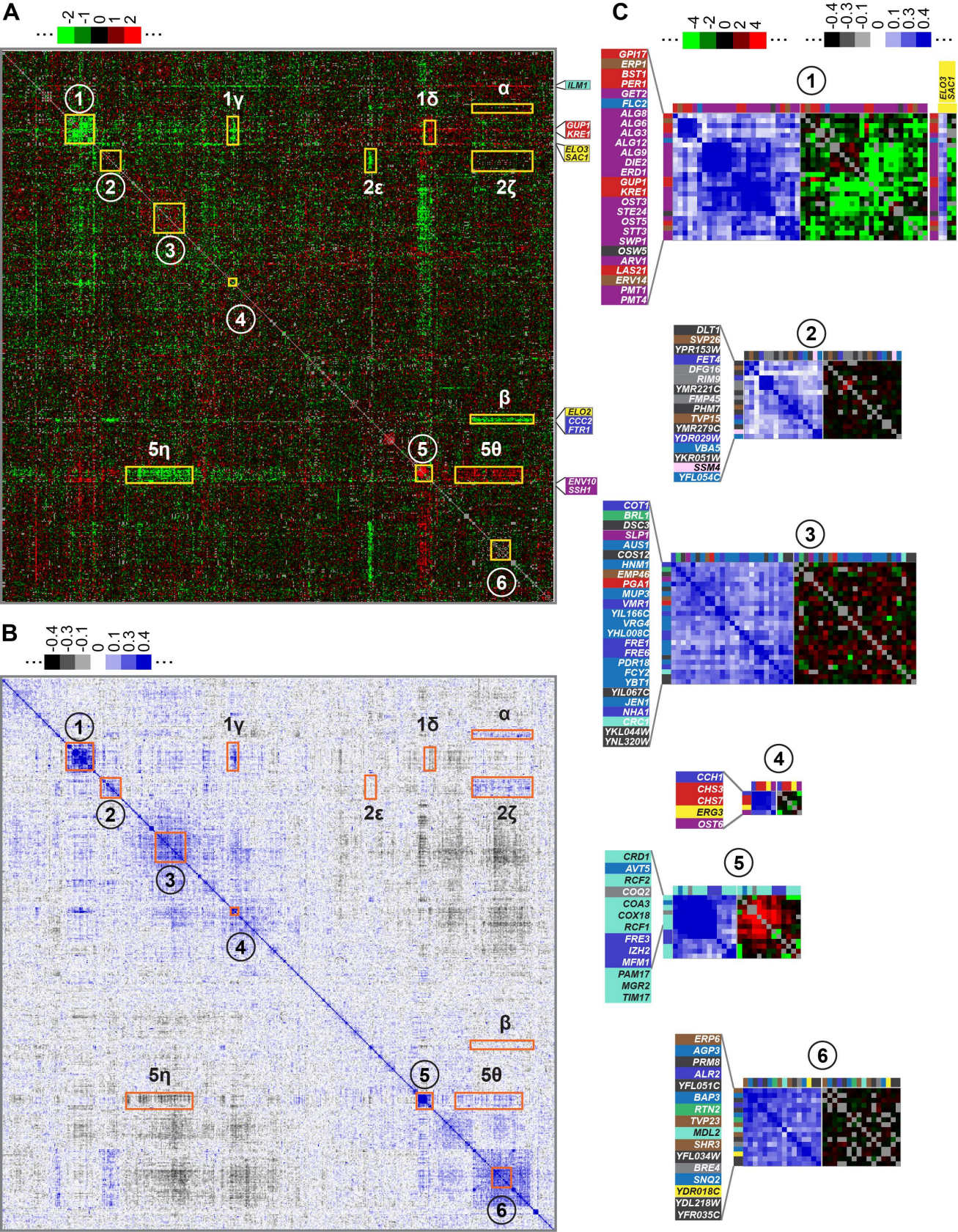
A
-2 -1 0 1 2
1
1γ
1δ
α
2ε
2ζ
2
3
4
β
5η
5
5θ
6
ILM1
GUP1
KRE1
ELO3
SAC1
ELO2
CCC2
FTR1
ENV10
SSH1
B
-0.4 -0.3 -0.1 0 0.1 0.3 0.4
C
-4 -2 0 2 4
-0.4 -0.3 -0.1 0 0.1 0.3 0.4
GPI17
ERP1
BST1
PER1
GET2
FLC2
ALG8
ALG6
ALG3
ALG12
ALG9
DIE2
ERD1
GUP1
KRE1
OST3
STE24
OST5
STT3
SWP1
OSW5
ARV1
LAS21
ERV14
PMT1
PMT4
ELO3
SAC1
DLT1
SVP26
YPR153W
FET4
DFG16
RIM8
YMR221C
FMP45
PHM7
TVP15
YMR279C
YDR029W
VBA5
YKR051W
SSM4
YFL054C
COT1
BRL1
DSC3
SLP1
AUS1
COS12
HNM1
EMP46
PGA1
MUP3
VMR1
YIL166C
VRG4
YHL008C
FRE1
FRE6
PDR18
FCY2
YBT1
YIL067C
JEN1
NHA1
CRC1
YKL044W
YNL320W
CCH1
CHS3
CHS7
ERG3
OST6
CRD1
AVT5
RCF2
COQ2
COA3
COX18
RCF1
FRE3
IZH2
MFM1
PAM17
MGR2
TIM17
ERP6
AGP3
PRM8
ALR2
YFL051C
BAP3
RTN2
TVP23
MDL2
SHR3
YFL034W
BRE4
SNQ2
YDR018C
YDL218W
YFR035C

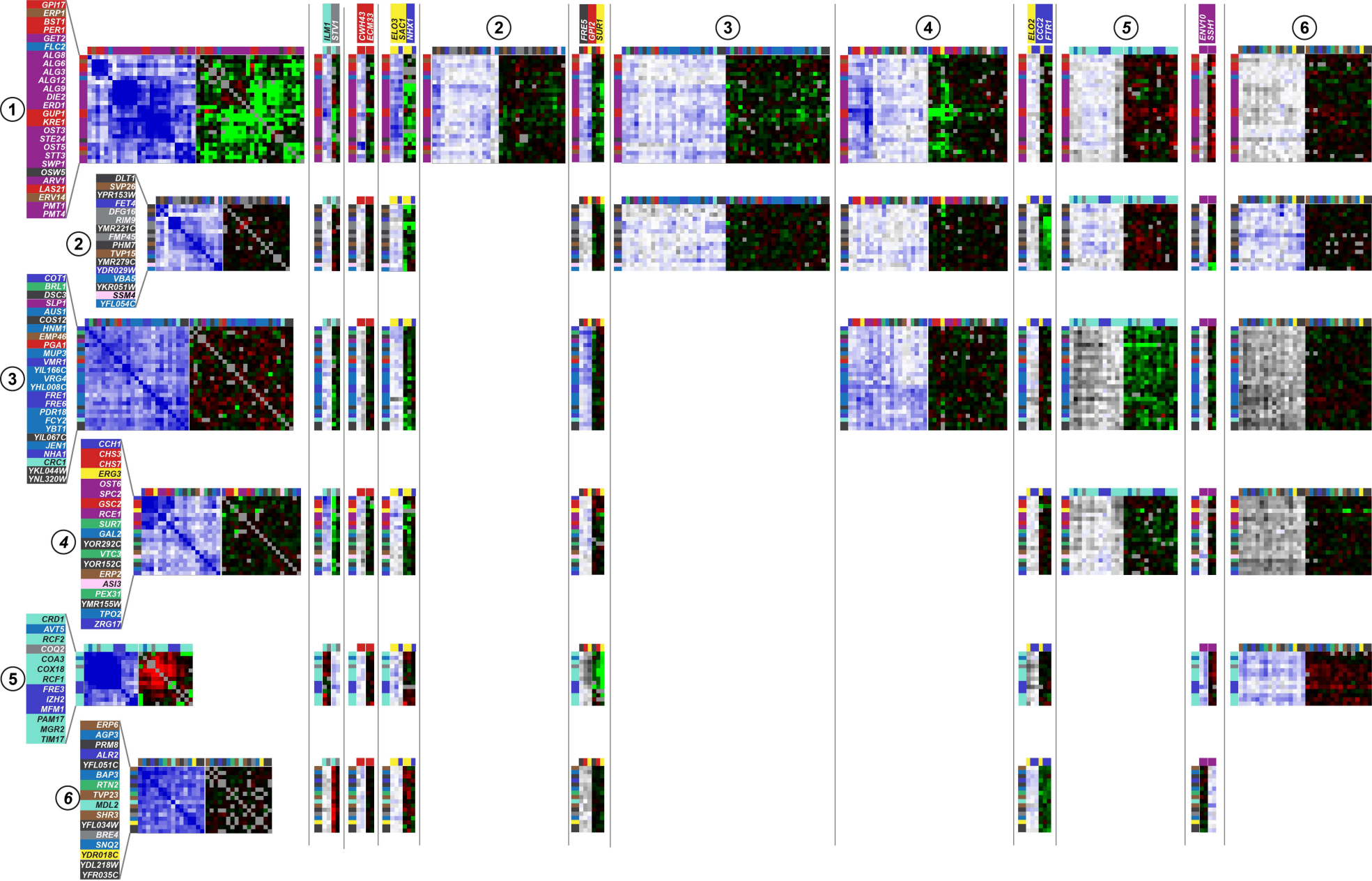
GPI17
ERP1
BST1
PER1
GET2
PLC2
ALG8
ALG6
ALG3
ALG12
ALG9
DIE2
ERD1
GUP1
KRE1
OST3
STE24
OST5
STT3
SWP1
OSW5
ARV1
LAS21
ERV14
PMT1
PMT4
1
ILM1
STV1
CWH43
EGH43
ELO3
SAC1
NPR1
2
FRE5
GPI2
SUR1
3
4
ELO2
CCC2
FTR1
5
ENV10
SSH1
6
DLT1
SVP26
YPR153W
FET4
DFG16
RIM9
YMR221C
FMP45
PHM7
TVP15
YMR279C
YDR029W
VBA5
YKR051W
SSM4
YFL054C
2
COT1
BRL1
DSC3
SLP1
AUS1
COS12
HNM1
EMP46
PGA1
MUP3
VMR1
YIL166C
VRG4
YHL008C
FRE1
FRE6
PDR18
FCY2
YBT1
YIL067C
JEN1
NHA1
CRC1
YKL044W
YNL320W
3
CCH1
CHS3
CHS7
ERG3
OST6
SPC2
GSC2
RCE1
SUR7
GAL2
YOR292C
VTC3
YOR152C
ERP2
ASI3
PEX31
YMR155W
TPO2
ZRG17
4
CRD1
AVT5
RCF2
COQ2
COA3
COX18
RCF1
FRE3
IZH2
MFM1
PAM17
MGR2
TIM17
5
ERP6
AGP3
PRM8
ALR2
YFL051C
BAP3
RTN2
TVP23
MDL2
SHR3
YFL034W
BRE4
SNQ2
YDR018C
YDL218W
YFR035C
6

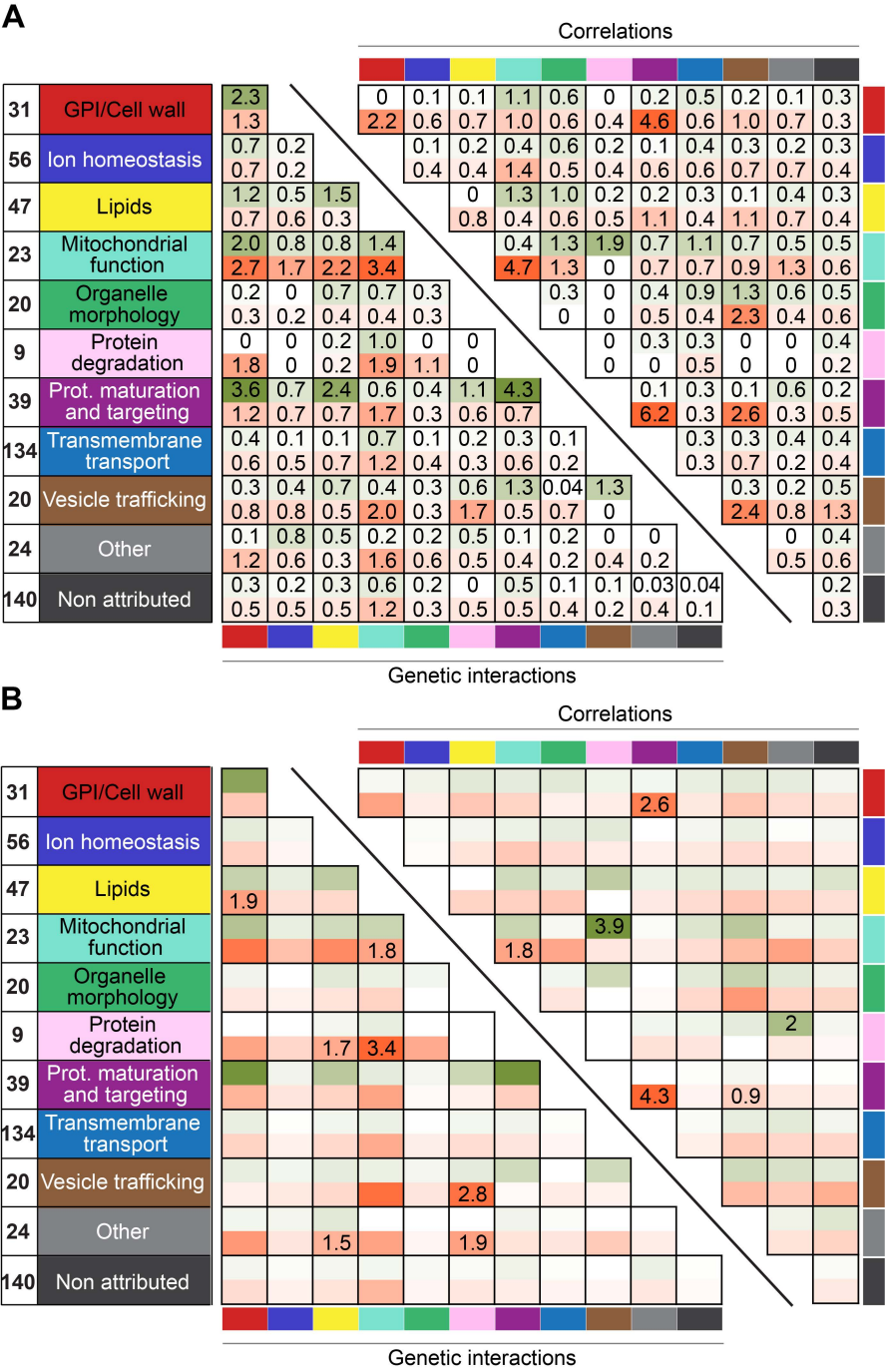
A
Correlations
31 GPI/Cell wall
56 Ion homeostasis
47 Lipids
23 Mitochondrial function
20 Organelle morphology
9 Protein degradation
39 Prot. maturation and targeting
134 Transmembrane transport
20 Vesicle trafficking
24 Other
140 Non attributed
Genetic interactions
B
Correlations
31 GPI/Cell wall
56 Ion homeostasis
47 Lipids
23 Mitochondrial function
20 Organelle morphology
9 Protein degradation
39 Prot. maturation and targeting
134 Transmembrane transport
20 Vesicle trafficking
24 Other
140 Non attributed
Genetic interactions

A

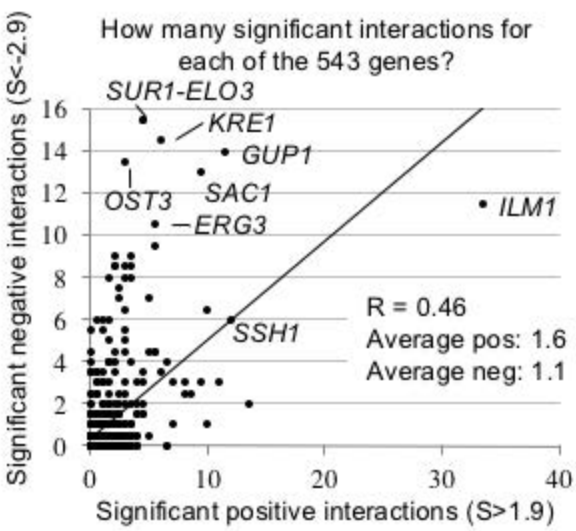

B

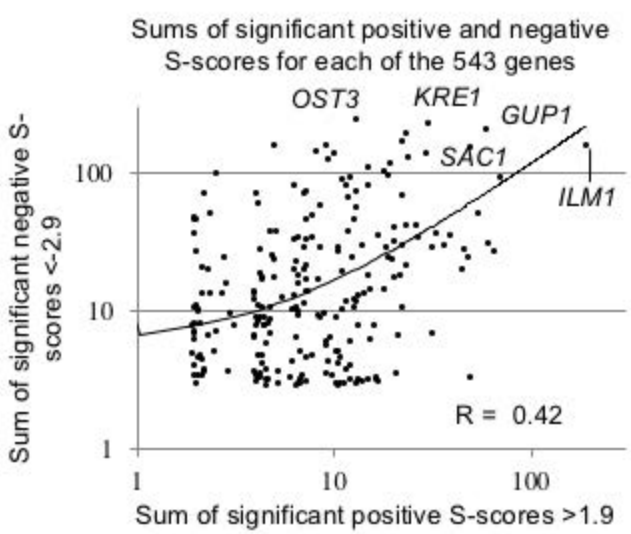

C

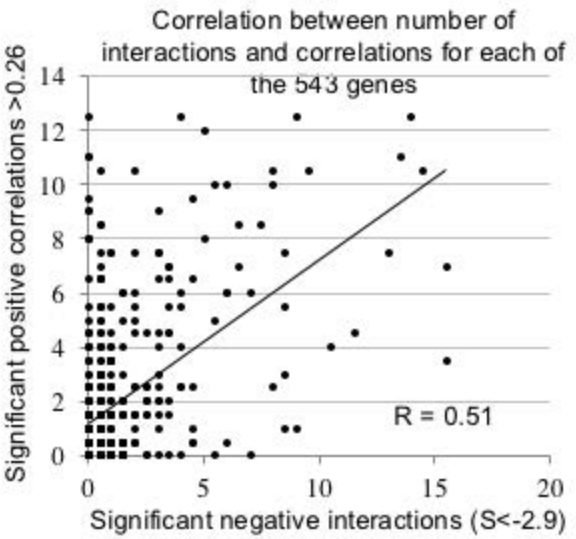

D

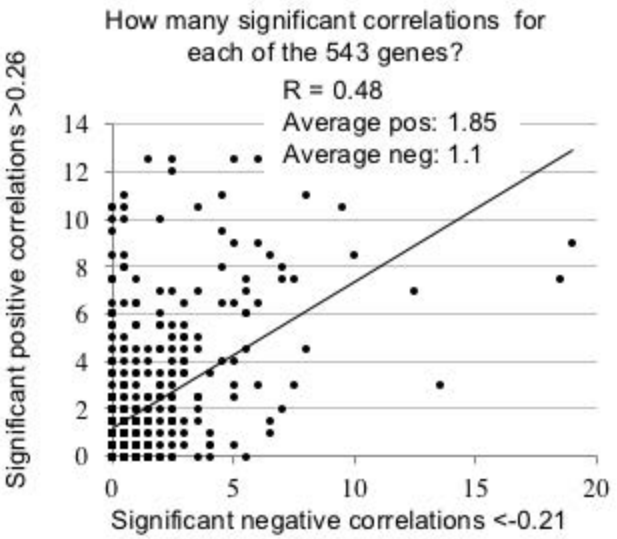

E

Correlations \ Interactions	None	Positive only	Negative only	Posit. and negat.	Sums
None	13	67	6	39	125
Positive only	7	42	6	70	125
Negative only	9	38	3	16	66
Posit. and negat.	9	85	13	120	227
Sums	38	232	28	245	

F

MSP-E-MAP

	pos. S sc.	neg. S sc.	pos. corr.	neg. corr.
pos. S score	N/A			
neg. S score	0.464	N/A		
pos. corr.	0.23	0.512	N/A	
neg. corr.	0.185	0.032	0.482	N/A

MSP/C-E-MAP

	pos. S sc.	neg. S sc.	pos. corr.	neg. corr.
pos. S score	N/A			
neg. S score	0.532	N/A		
pos. corr.	0.191	0.155	N/A	
neg. corr.	0.043	0.057	0.151	N/A

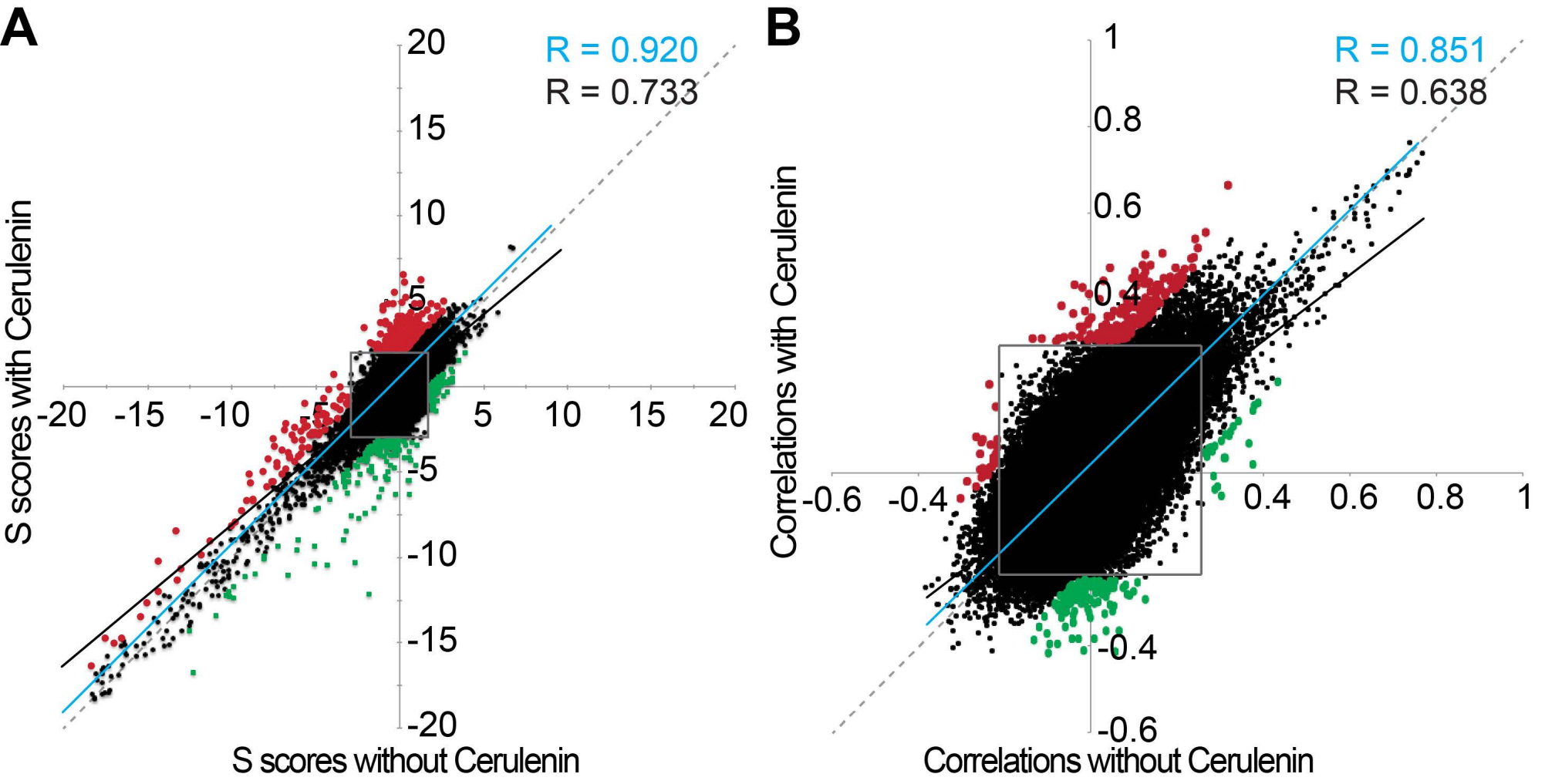
A
R = 0.920
R = 0.733
S scores with Cerulenin
S scores without Cerulenin
20
15
10
5
-5
-10
-15
-20
-20
-15
-10
-5
5
10
15
20
B
R = 0.851
R = 0.638
Correlations with Cerulenin
Correlations without Cerulenin
1
0.8
0.6
0.4
-0.4
-0.6
-0.6
-0.4
0.4
0.6
0.8
1

0 µg/ml Cerulenin

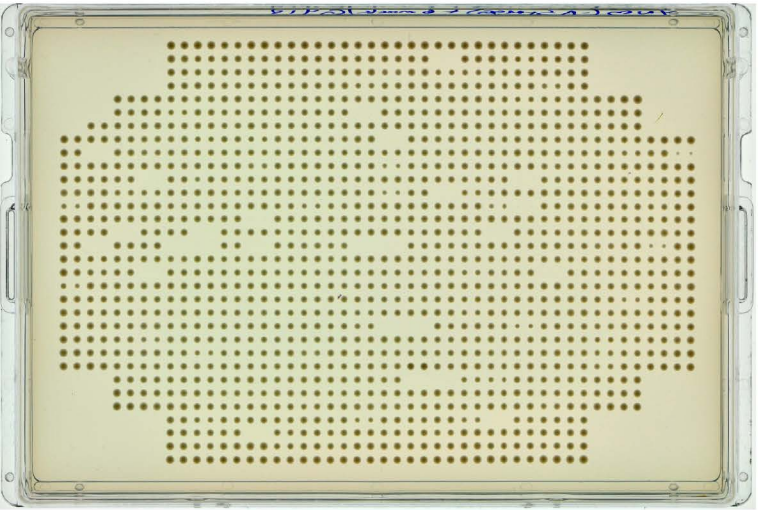

0.4 µg/ml Cerulenin

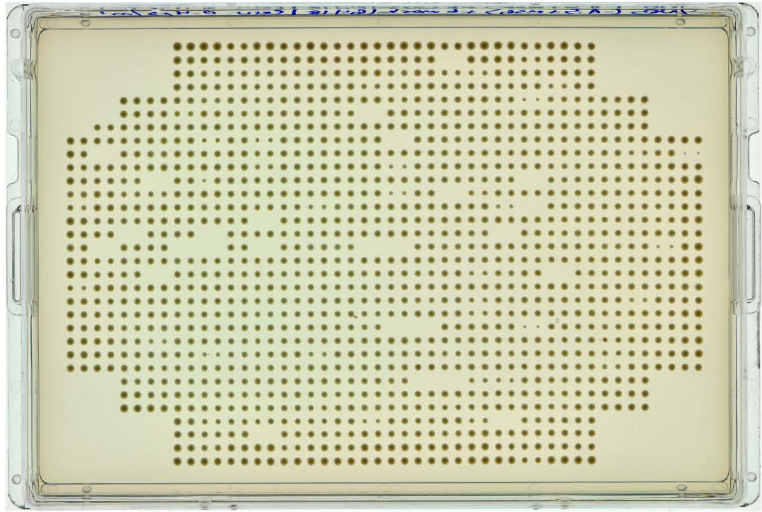

0.5 µg/ml Cerulenin

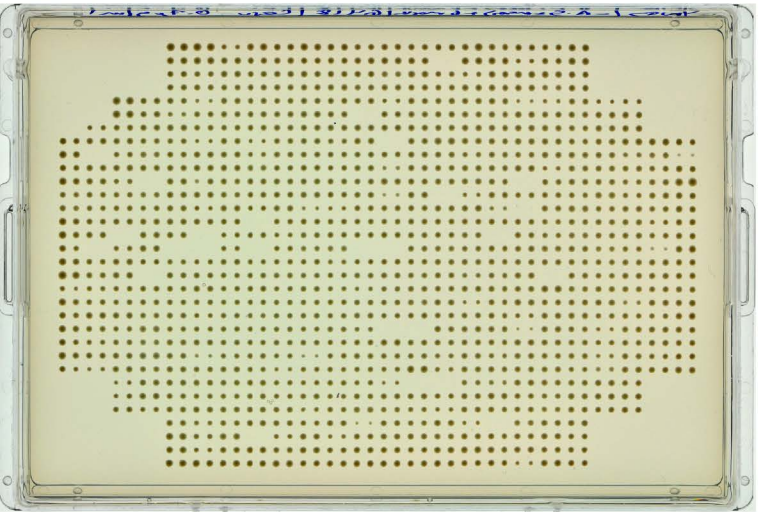

0.6 µg/ml Cerulenin